Chapter 16
Thermal Radiation Physics and Modeling

Symbols and Terminology

Subscripts

a	Absorber (absorbed)
alb	Albedo
B	Body under consideration
E	Earth
eff	Effective (temperature)
ext	External (to satellite)
int	Internal (to satellite)
IR	Infrared
r	Receiver (received)
S	Solar
sat	Satellite
sol	Solar
t	Transmitter (transmitted)
λ	Spectral
Ω	Directional
$\bullet$	Black body
$\perp$	(Surface) projection onto a given direction

Latin Symbols

a	Albedo
A	Size of surface area
E	Irradiance
$F_{i\to j}$	View factor (a.k.a. configuration factor) from surface i to surface j
G_{ij}	Heat conduction or heat convection coefficient (a.k.a. conductor) between node i and j
h	Planck constant

U. Walter, *Astronautics*, https://doi.org/10.1007/978-3-319-74373-8_16

I_Ω	Radiant intensity (directional)
k_B	Boltzmann constant
L_Ω	Radiance (directional)
$L_{\lambda\Omega}$	Spectral radiance (directional)
M	Radiant exitance
M_λ	Spectral exitance
Q	Radiant energy
R	Radiative conduction coefficient
s	Distance between emitting and absorbing surface points
S/C	Spacecraft

Greek Symbols

α	Absorptivity (*a.k.a.* absorption coefficient)
ε	Emissivity (*a.k.a.* emission coefficient, emittance)
θ	Polar angle (see Fig. 16.1)
λ	Wavelength
Φ	Radiant flux (*a.k.a.* radiative heat flux)
σ	Stefan-Boltzmann constant
Ω	Solid angle

Abbreviations

BOL	Beginning of life
CFRP	Carbon fiber reinforced plastics
ECSS	European cooperation for space standardization
EOL	End of life
FDM	Finite differences model
FEM	Finite element model
GMM	Geometrical mathematical model
IR	Infrared
ISS	International space station
MLI	Multi-layer insulation
OSR	Optical surface reflector
PCB	Printed circuit board
RHU	Radioisotope heater units
RTG	Radioisotope thermoelectric generator
S/C	Spacecraft
SSM	Second surface mirror
TCS	Thermal control system
TMM	Thermal mathematical model
TRP	Temperature reference point

Glossary for Thermal Modeling

Terms (TM = Thermal Model)

TM-specific term (here: CAPITAL LETTERS)	TM symbol	Conventional term (here: regular letters)	Conventional symbol
CONDUCTANCE		Coupling coefficient	
Linear CONDUCTOR	G_L	Coupling coefficient	G_{ij}
Fluid CONDUCTOR	G_F	Coupling coefficient	G_{ij}
Radiative CONDUCTOR	G_R	Coupling coefficient	R_{ij}
CONTACT CONDUCTANCE		Coupling coefficient	
CAPACITANCE or thermal capacity	C	Heat capacity	C
Heat flux	Q	Heat flux	Φ

The ultimate goal of this chapter is to determine the temperature equilibrium distribution inside a spacecraft (S/C) as a result of the thermal equilibrium with its space environment. Knowing these inside temperatures is essential when designing a S/C, as most components only work reliably within certain temperature ranges: batteries loose capacity and propellants may freeze.

The heat exchange and thermal balance problem of the S/C can be split into a S/C internal and external one, which must be also in equilibrium with each another. An internal thermal balance analysis covers the heat exchanged between the passive parts and surfaces within the S/C, as well as internal heat sources like heaters, batteries etc. This internal heat balance is complemented by the external one as the S/C interacts with external heat sources (Sun, planets, etc.) and sinks (deep space). The boundary between those two "cavities" is the outer hull of the S/C.

In Sect. 16.1 we start out with the radiometric concepts of radiation and the physics of some idealized radiation surfaces. Then we look in Sect. 16.2 at the radiation exchange between surfaces and how to possibly affect it, before we finally come in Sect. 16.3 to the thermal modeling and simulation as the basis for thermal spacecraft design.

16.1 Radiation Properties

Let us first start with the external heat balance. It is driven by the radiative heat exchange of the outer S/C surfaces with the environment. On the one hand these surfaces can absorb heat in different wavelengths, while on the other they emit heat, usually in the infra-red (IR) range. There are three key sources for the heat flux onto a S/C that is in an orbit in proximity to a planet: direct sunlight, sunlight reflected by the planet (albedo), and infrared radiation (IR) from the planet. As the density of Earth's atmosphere in space is extremely low, there is almost no heat transfer by

heat convection. The only transfer mechanism between the S/C and the environment is thermal radiation.

For the sake of analytical simplicity let us assume for now that the S/C is isothermal, i.e. that it has a uniform surface temperature and that the S/C is in thermal equilibrium, so there is more or less the same temperature everywhere within the S/C. If this is not the case, our calculations are valid for the thermally averaged S/C. In this way let us have a look at the thermal radiation heat transfer.

16.1.1 Radiometric Concepts

When radiation is transferred, electromagnetic waves (photons), each with energy $E_v = hv$, where h is Planck's constant and ν its frequency, are emitted and transmitted by a radiator (subscript t) to an absorbing receiver (subscript r). These indices are consistent with those in radio and microwave technology. In the following, rather than photometric notation we will use radiometric notation and nomenclature, which is more common in thermal radiation analysis.

Photon Flux
The total number N of photons that are emitted, reflected, or received by a surface is the so-called *radiant energy*

$$Q = N \cdot E_v \ [\mathrm{J}] \quad \textbf{radiant energy} \tag{16.1.1}$$

measured in joule $[\mathrm{J}] = [\mathrm{W} \cdot \mathrm{s}]$. The radiant energy per time unit dt is called the *radiant flux* (a.k.a. *radiative heat flux*)

$$\Phi := \frac{dQ}{dt} \ [\mathrm{W}] \quad \textbf{radiant flux} \tag{16.1.2}$$

The radiant flux is the only physically relevant quantity for thermal radiation, because it describes the total flow of photons per time unit. So, it is the photon flux in question and hence is the starting point for all further considerations.

> **Note** *The radiometric term flux used here is not consistent with flux in the physics of transport phenomena (heat transfer, mass transfer, and fluid dynamics), where flux is defined as the rate of flow of a quantity per unit area.*

Photons may have different wavelengths λ and may flow in different directions $\Omega = (\theta, \varphi)$ (see Fig. 16.1). Therefore, we differentiate the photon flux into a flux density per $d\lambda$, $d\Omega$, and $dA_{t,\perp}$ of an emitting, receiving, or reflecting, surface

$$d^3\Phi = L_{\lambda\Omega} \cdot d\lambda \, d\Omega \, dA_{\perp} \tag{16.1.3}$$

where the flux density $L_{\lambda\Omega}$ is the so-called *spectral radiance* (a.k.a. *spectral luminance* (in photometry) or *spectral (radiation) intensity*)

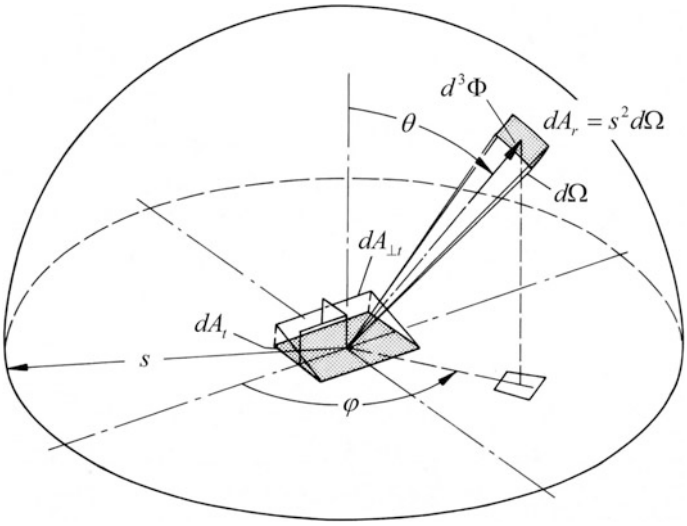

Fig. 16.1 Unit surface area dA_t transmitting radiant flux $d^3\Phi$ into direction $\Omega = (\theta, \varphi)$ (θ = polar angle) with aperture angle $d\Omega$, and an infinitesimal receiving surface $dA_r = s^2 d\Omega$ at distance s

$$L_{\lambda\Omega}(\lambda, \Omega) := \frac{d^3\Phi}{d\lambda\, d\Omega\, dA_\perp} \quad \left[\frac{W}{m^2\, sr\, \mu m}\right] \quad \textbf{spectral radiance} \qquad (16.1.4)$$

The subscripts λ and Ω indicate the corresponding density. It is crucial to this definition that the radiance is defined per dA projected onto the transmitting or receiving direction, i.e. per

$$dA_\perp = dA \cdot \cos\theta$$

where θ is the polar angle of the radiation's direction (see Fig. 16.1).

In summary, The basic physical quantity $d^3\Phi$ describes a photon flux having wavelength λ, flowing in direction $\Omega = (\theta, \varphi)$, and being related to any given projected surface $dA_\perp$ that emits, reflects, or receives the radiation.

Terminology and Notations

- When sloppily saying "the radiation", we actually mean, here and in the following, the important quantity $d^3\Phi$, the differential photon flux.
- All photon-flux-derived quantities (above and in the following) are defined relative to a differential (emitting, receiving, or reflecting) surface area dA (as part of a possibly total radiating body). Hence, dA can radiate only into the hemisphere above it, indicated by the symbol $\cap$.

- Quantities that are derived by integration over all directions hence will sometimes be termed "hemispherical" and those derived by integration over all wavelengths as "total".
- Spectral (λ) and/or directional (Ω) densities, such as $L_{\lambda\Omega}(\lambda, \Omega)$, generally have according spectral and directional dependencies. We therefore will furthermore drop the dependency specification (λ, Ω) and just write $L_{\lambda\Omega}$. In the case when a relevant dependency does not apply, we cross it out, e.g. $L_{\Omega}(\not{\Omega})$ for a directionally independent radiance.
- We sometimes will make use of the more compact notation of integrals

$$[f(\lambda)]_{\lambda} := \int_0^{\infty} f(\lambda) \cdot d\lambda, \quad [f(\theta, \varphi)]_{\Omega} := \int_{\cap} f(\theta, \varphi) \cdot d\Omega$$

Surface-Specific Radiation Densities

Obviously, the transmitted radiation $d^3\Phi_t$ must be proportional to and dependent on the emitting surface area of the radiator. Therefore, radiometry defines the so-called *radiant exitance* (a.k.a, *emissive power*) M as

$$M := \frac{d\Phi_t}{dA_t} \left[\frac{W}{m^2}\right] \quad \textbf{radiant exitance} \tag{16.1.5}$$

Note that in contrast to radiance, exitance is defined per actual emitting unit surface area dA_t. Because by definition M applies only for transmitting (emitting) surfaces, its subscript t is always dropped. Most generally, the so-called *spectral and directional radiant exitance* is defined as

$$M_{\lambda\Omega} := \frac{d\Phi_t}{d\lambda\, d\Omega_t\, dA_t} \left[\frac{W}{m^2\, sr\, \mu m}\right] \tag{16.1.6}$$

By comparison with Eq. (16.1.4) and because $dA_{\perp} = dA \cdot \cos\theta$ we find

$$M_{\lambda\Omega} = L_{\lambda\Omega,t} \cos\theta_t \tag{16.1.7}$$

Another prominent quantity is the *spectral (radiant) exitance*

$$M_{\lambda} := \frac{dM}{d\lambda} \left[\frac{W}{m^2 \mu m}\right] \quad \textbf{spectral exitance} \tag{16.1.8}$$

By the same token we define the quantity *irradiance*, which is the radiant flux incident on a receiving unit area

$$E := \frac{d\Phi_r}{dA_r} \quad \textbf{irradiance} \tag{16.1.9}$$

By definition, E applies only for receiving surfaces, which is why its subscript r is also dropped regularly. By the same token as above we have

$$E_{\lambda\Omega}(\lambda, \Omega) = L_{\lambda\Omega,r} \cos\theta_r \tag{16.1.10}$$

Total Directional Radiation

For thermal radiation exchange between two surfaces, to which we come later, only the total and not the spectral exchanged photon flux is of interest. This results in directional flux densities, which are integral in λ and are therefore sometimes called "total".

So, for an emitting, reflecting, or receiving surface element $dA_\perp$ and in accordance with Eq. (16.1.4) we have the so-called *radiance* (a.k.a. *luminance* (in photometry) or *radiation intensity*)

$$L_\Omega := \frac{d^2\Phi}{d\Omega \cdot dA_\perp} \left[\frac{W}{m^2 sr}\right] \quad \textbf{radiance} \tag{16.1.11}$$

For a given emitting surface this directional photon flux density in total defines the fraction of hemisphere above the surface that receives the incoming irradiation (cf. Fig. 16.1). This is the significance of the quantity *radiation*.

Another directional quantity is the so-called *radiant intensity* (a.k.a. *total intensity*) defined as the radiant flux per solid angle Ω

$$I_\Omega(\Omega) := \frac{d\Phi}{d\Omega} \left[\frac{W}{sr}\right] \quad \textbf{radiant intensity} \tag{16.1.12}$$

In conclusion, we find from Eqs. (16.1.5), (16.1.12), and (16.1.11) and with $dA_\perp = dA \cdot \cos\theta$

$$\frac{dM}{d\Omega_t} = \frac{dI_{\Omega,t}}{dA_t} = L_{\Omega,t} \cos\theta_t \quad @ \text{ transmitter} \tag{16.1.13}$$

$$\frac{dE}{d\Omega_r} = \frac{dI_{\Omega,r}}{dA_r} = L_{\Omega,r} \cos\theta_r \quad @ \text{ receiver} \tag{16.1.14}$$

16.1.2 Diffuse Radiators

Although all real radiators exhibit wavelength-dependent emission and absorption, there are many radiators, particular those with very rough surfaces, showing nearly direction-independent (isotropic) emission and absorption. Therefore, assuming isotropic radiator properties is often a good approximation. This is widely utilized

and will be essential for radiation exchange in Sect. 16.2.1. Isotropic radiation is also called *diffuse radiation* and a diffusely emitting surface accordingly is called a *diffuse radiator, diffuse surface,* or *Lambertian surface*.

What are the radiation properties of a diffuse surface? According to Eq. (16.1.7) for every radiator $M_{\lambda\Omega} = L_{\lambda\Omega,t} \cos\theta_t$ holds. If a surface radiates isotropically (diffusively), then $L_{\lambda\Omega,t}(\not{\Omega})$, meaning $L_{\lambda\Omega,t}$ is independent of direction Ω i.e., it has the same radiance when viewed from any angle. We thus can write

$$M_{\lambda\Omega} = L_{\lambda\Omega,t}(\not{\Omega}) \cos\theta_t \quad @ \text{ diffuse} \quad \textbf{Lambert's cosine law} \tag{16.1.15}$$

This is the so-called *Lambert's cosine law*. We recall that the $\cos\theta$ dependence is merely of geometrical origin, namely due to the fact that $dA_\perp = dA \cdot \cos\theta$.

We now integrate Lambert's cosine law over a hemisphere and make use of the isotropy:

$$M_\lambda = \int_\cap M_{\lambda\Omega} \cdot d\Omega = \int_\cap L_{\lambda\Omega}(\not{\Omega}) \cos\theta \cdot d\Omega = L_{\lambda\Omega}(\not{\Omega}) \int_\cap \cos\theta \cdot d\Omega$$

Because $d\Omega = \sin\theta \cdot d\theta \cdot d\varphi$, the last integration delivers

$$\int_\cap \cos\theta \cdot d\Omega = \int_0^{\pi/2} \int_0^{2\pi} d\varphi \cdot \cos\theta \sin\theta \cdot d\theta = 2\pi \left(\frac{1}{2} \sin^2\theta \right) \Big|_0^{\pi/2} = \pi$$

So, the integral does not result in the solid angle of a hemisphere, 2π, but only in π, because the effective radiation surface $dA_\perp = dA \cdot \cos\theta$ decreases with increasing polar angle, thus diminishing the exitance towards the azimuthal plane. We therefore obtain for a diffuse radiator

$$M_\lambda = \pi \cdot L_{\lambda\Omega}(\not{\Omega}) \quad @ \text{ diffuse} \tag{16.1.16a}$$

and by integration over all wavelengths finally

$$M = \pi \cdot L_\Omega(\not{\Omega}) \quad @ \text{ diffuse} \tag{16.1.16b}$$

Observe that directional density L_Ω is in units $[\mathrm{W}/(\mathrm{m}^2 sr)]$ and π in $[sr]$, which correctly delivers M in $[\mathrm{W}/\mathrm{m}^2]$. According to Eq. (16.1.14), a diffuse surface hence emits the radiant intensity

$$I_\Omega(\not{\Omega}) = \int L_\Omega(\not{\Omega}) \cos\theta_t \cdot dA_t = \frac{M}{\pi} \int \cos\theta_t \cdot dA_t$$

By defining

$$A_\perp := \int_A \cos\theta \cdot dA \quad \text{effective (projected) surface} \tag{16.1.17}$$

we obtain

$$I_\Omega(\not{\Omega}) = \frac{M}{\pi} A_{\perp,t} \quad @ \text{ diffuse} \tag{16.1.18}$$

16.1.3 Black-Body Radiator

Spectral and directional exitance is key for thermal radiation physics. By definition, a so-called *black-body radiator* (subscript •) is a radiator (radiating body, surface or surface element) with the following idealized spectral and directional properties:

1. A black body absorbs all incident radiation, regardless of wavelength and direction.
2. At a given temperature and wavelength no body emits more energy than a black body.
3. A black body is a diffuse radiator, i.e. the emitted radiation and hence $L_{\lambda\Omega,\bullet}(\not{\Omega})$ is independent of direction (indicated by $\not{\Omega}$).

Because the black body is a diffuse radiator, all results from Sect. 16.1.2 apply.

Owing to internal statistical quantum processes in thermal equilibrium the absorbed radiation is reemitted with a characteristic spectral distribution, to which we come in a moment. For instance, a black-body at room temperature will absorb all visible sunlight and turn it into an infrared (IR) radiation spectrum. Because IR radiation is outside the visible range, such a black body will look totally black from outside—the reason it has been given that name. A black body is an idealization in most cases. But as we will see in the upcoming Sect. 16.1.4 real radiators and absorbers can be traced back to a black-body by means of correction factors. This is why the physics of a black-body radiator is so important. Let us have a closer look at it.

In 1900 the famous physicist Max Planck was able to show—for which he later got a Nobel prize—that the spectral exitance of a black-body radiator can be written as

$$M_{\lambda,\bullet} := \frac{dM_\bullet}{d\lambda} = \frac{2\pi hc^2}{\lambda^5}\left[\exp\left(\frac{hc}{\lambda k_B T}\right) - 1\right]^{-1} \quad \textbf{Planck's law} \tag{16.1.19}$$

with c the velocity of light, k_B Boltzmann constant, and h Planck's constant. It is depicted in Fig. 16.2. The substitution

$$x := \frac{hc}{\lambda k_B T}$$

yields the normalized form

$$M_{\lambda,\bullet} = \frac{2\pi k_B^5 T^5}{c^3 h^4} \frac{x^5}{e^x - 1}$$

Observe that it has the consistent shape $x^5/(e^x - 1)$, and it is merely stretched in size by T^5. So, $M_{\lambda,\bullet}$ has a consistent maximum at $x_{\max} = 4.965114232\ldots$

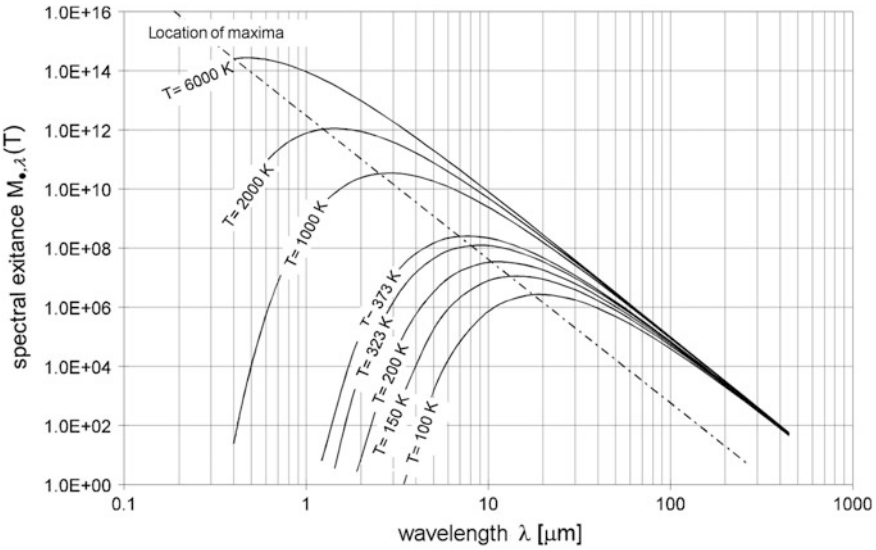

Fig. 16.2 The spectral exitance $M_{\lambda,\bullet}$ of a black body as a function of wavelength and for different body temperatures

(see Problem 16.1) and thus

$$\lambda_{\max} \cdot T = \frac{hc}{k_B x_{\max}} = 2897.752\ \mu\text{m} \cdot \text{K} \quad \textbf{Wien's displacement law} \qquad (16.1.20)$$

Example

The radiation temperature of the Sun is $T = 5778$ K and its spectral maximum hence is at $\lambda_{\max} = 502$ nm (*green light*). Earth on the other hand radiates at temperature $T = 254$ K (see Problem 16.2), which corresponds to a radiation maximum at $\lambda_{\max} = 11.4$ μm, i.e. infrared radiation.

Remark *The variable $x = hc/\lambda k_B T = h\nu/k_B T$, with photon frequency ν, actually has physical relevance: The energy of a photon is $E_\nu = h\nu$ and thus $E_\nu = x(\nu)k_B T$. Therefore, most photons are radiated with the energy $E_{\max} = x_{\max} k_B T \approx 5 k_B T$. But, as the function $x^5/(e^x - 1)$ is strongly asymmetrical, $E_{\max}$ does not correspond to the mean energy E_{ave} of all emitted photons, but rather $E_{ave} = 3.83\ k_B T$. In other words: A black-body radiator at temperature T has internal energy $k_B T$ and thus generates photons with mean energy 3.83 $k_B T$, i.e. of order $k_B T$. So a black-body radiates its internal energy $k_B T$ away by photons of the same energy.*

For the radiant exitance of a black body we find with the help of mathematical tables

$$M_\bullet = \int_0^\infty M_{\lambda,\bullet} \cdot d\lambda = \frac{2\pi k_B^4 T^4}{c^2 h^3} \int_0^\infty \frac{x^3}{e^x - 1} \cdot dx = \frac{2\pi k_B^4 T^4}{c^2 h^3} \frac{\pi^4}{15}$$

Hence

$$\boxed{M_\bullet = \sigma T^4} \quad \textbf{Stefan–Boltzmann law} \tag{16.1.21}$$

with

$$\sigma := \frac{2\pi^5 k_B^4}{15 c^2 h^3} = 5.670400 \times 10^{-8} \frac{\mathrm{W}}{\mathrm{m}^2\ \mathrm{K}^4} \quad \textbf{Stefan–Boltzmann constant}$$

The Stefan-Boltzmann law is an important result, which we will make use of frequently in the upcoming sections.

Since a black body is a diffuse radiator, we derive from Eq. (16.1.16b)

$$M_\bullet = \pi L_{\Omega,\bullet}(\not{\Omega}) = \sigma T^4 \tag{16.1.22}$$

16.1.4 Selective Surfaces

Real radiators generally differ from the ideal of a black-body radiator by being spectrally selective and also differ from a diffuse surface by being directionally selective.

Emitting Surfaces

Based on the properties of a black body, spectrally and directionally selective emitting surfaces can be described as surfaces that modulate the ideal spectral radiance of a black-body radiator by a characteristic emission factor, the so-called *directional spectral emissivity* (a.k.a. *directional spectral emission coefficient*), defined by

$$\varepsilon_{\lambda\Omega}(T) := \frac{L_{\lambda\Omega,t}}{L_{\lambda\Omega,\bullet}} \leq 1 \quad \textbf{directional spectral emissivity} \tag{16.1.23}$$

Note that $\varepsilon_{\lambda\Omega}(T)$ is dimensionless and generally temperature-dependent. From this definition we derive with Eq. (16.1.7)

$$M_{\lambda\Omega,t} = \varepsilon_{\lambda\Omega} L_{\lambda\Omega,\bullet}(\not{\Omega}) \cos\theta_t \tag{16.1.24}$$

Because for further thermal radiation exchange between surfaces only directional spectral radiation flow is of interest, we define the *directional total emissivity* as

$$\varepsilon_\Omega(T) := \frac{L_{\Omega,t}}{L_{\Omega,\bullet}} = \frac{\pi}{\sigma T^4} \int_0^\infty \varepsilon_{\lambda\Omega} L_{\lambda\Omega,\bullet}(T) \cdot d\lambda \le 1 \quad \begin{matrix}\textbf{directional}\\ \textbf{total emissivity}\end{matrix} \tag{16.1.25}$$

where the latter follows from Eq. (16.1.22). We further define the important relation

$$\boxed{M =: \varepsilon(T) \cdot M_\bullet = \varepsilon(T) \cdot \sigma\, T^4} \tag{16.1.26}$$

This determines the *hemispherical total emissivity*, which reads with Eqs. (16.1.24) and (16.1.25) (for the notation $[\ldots]_x$ see insert *Terminology and Notations* in Sect. 16.1.1) after Eq. (16.1.4))

$$\varepsilon(T) := \frac{M}{M_\bullet} = \frac{1}{M_\bullet} \left[\left[\varepsilon_{\lambda\Omega} L_{\lambda\Omega,\bullet}(\Omega) \cos\theta_t \right]_{\Omega_t} \right]_\lambda < 1 \quad \begin{matrix}\textbf{hemispherical}\\ \textbf{total emissivity}\end{matrix}$$

This can be transposed either as

$$\varepsilon(T) = \frac{1}{M_\bullet} \left[\left[\varepsilon_{\lambda\Omega} \cos\theta_t \right]_{\Omega_t} L_{\lambda\Omega,\bullet} \right]_\lambda = \frac{1}{M_\bullet} \left[\varepsilon_\lambda L_{\lambda\Omega,\bullet} \right]_\lambda$$

or

$$\varepsilon(T) = \frac{1}{M_\bullet} \left[\left[\varepsilon_{\lambda\Omega} L_{\lambda\Omega,\bullet} \right]_\lambda \cos\theta_t \right]_{\Omega_t} = \frac{1}{M_\bullet} \left[\varepsilon_\Omega L_{\Omega,\bullet}(\Omega) \cos\theta_t \right]_{\Omega_t} = \frac{L_{\Omega,\bullet}}{M_\bullet} \left[\varepsilon_\Omega \cos\theta_t \right]_{\Omega_t}$$

From the latter we finally obtain with $M_\bullet = \pi\, L_{\Omega,\bullet}$ (see Eq. (16.1.22))

$$\varepsilon(T) = \frac{1}{\pi} \int_\cap \varepsilon_\Omega(T) \cos\theta_t \cdot d\Omega_t \le 1 \tag{16.1.27}$$

Absorbing Surfaces

Equivalently, the radiant flux $d^2\Phi_a$ absorbed by a body is not the entire received radiant flux $d^2\Phi_r$ (as for a black body), but is a spectrally and directionally selective fraction, $\alpha_{\lambda\Omega}$, of that. This fraction is named *directional spectral absorptivity* (a.k.a. *directional spectral absorption coefficient*)

$$\alpha_{\lambda\Omega}(T) := \frac{d^3\Phi_a}{d^3\Phi_r} = \frac{L_{\lambda\Omega,a}}{L_{\lambda\Omega,r}} = \frac{E_{\lambda\Omega,a}}{E_{\lambda\Omega,r}} \le 1 \quad \begin{matrix}\textbf{directional}\\ \textbf{spectral absorptivity}\end{matrix} \tag{16.1.28}$$

where the latter identities follow from Eqs. (16.1.4) to (16.1.10). Note that $\alpha_{\lambda\Omega}(T)$, like $\varepsilon_{\lambda\Omega}(T)$, is dimensionless and generally also temperature-dependent. The subscripts just indicate the spectral and directional dependences.

By the same token as for the emissivity we define the *directional total absorptivity* as

$$\alpha_\Omega(T) := \frac{L_{\Omega,a}}{L_{\Omega,r}} = \frac{\left[L_{\lambda\Omega,a}\right]_\lambda}{\left[L_{\lambda\Omega,r}\right]_\lambda} = \frac{\left[\alpha_{\lambda\Omega} L_{\lambda\Omega,r}\right]_\lambda}{\left[L_{\lambda\Omega,r}\right]_\lambda} \le 1 \quad \begin{matrix}\textbf{directional}\\ \textbf{total absorptivity}\end{matrix} \tag{16.1.29}$$

(for the notation $[\ldots]_x$ see insert *Terminology and Notations* in Sect. 16.1.1 after Eq. (16.1.4)) and the *hemispherical total absorptivity* as

$$\alpha(T) := \frac{E_a}{E_r} = \frac{\left[\left[\alpha_{\lambda\Omega} L_{\lambda\Omega,r}\right]_\lambda \cos\theta_r\right]_\Omega}{\left[\left[L_{\lambda\Omega,r}\right]_\lambda \cos\theta_r\right]_\Omega} \le 1 \quad \begin{matrix}\textbf{hemisperical}\\ \textbf{total absorptivity}\end{matrix} \tag{16.1.30}$$

With Eq. (16.1.29) we derive

$$\alpha = \frac{\left[\left[\alpha_{\lambda\Omega} L_{\lambda\Omega,r}\right]_\lambda \cos\theta_r\right]_\Omega}{\left[\left[L_{\lambda\Omega,r}\right]_\lambda \cos\theta_r\right]_\Omega} = \frac{\left[\alpha_\Omega L_{\Omega,r} \cos\theta_r\right]_\Omega}{\left[L_{\Omega,r} \cos\theta_r\right]_\Omega}$$

Equation (16.1.30) can we written with Eq. (16.1.9) as

$$d^2\Phi_a = \alpha(T_t) \cdot d^2\Phi_r \tag{16.1.31}$$

Observe that the total absorptivity depends on the received spectral distribution and hence on the temperature of the transmitter (radiator) and not on that of the absorber.

Real Radiators and Absorbers

Spectrally selective surfaces are the rule. Figure 16.3 for instance shows the spectral absorptivity of some metals and paints used in S/C thermal design. In particular the emissivity of metallic surfaces is reduced due to their strong absorption with an absorption edge in the infrared (see Fig. 16.3) and varies drastically depending on the type of metal and its surface properties (e.g. oxidation).

Most dielectric materials and metals have also directionally selective surfaces. Figure 16.4 shows typical angle-dependent emission figures.

If surfaces are no longer smooth (i.e. roughness > wavelength ≈ 0.5 μm) as assumed so far, or if they are oxidized, contaminated, or even painted, their emissivity and absorptivity may exhibit quite different values. They also show a strong dependency on brightness, wavelength and temperature. For $T < 500$ K and $\lambda > 5$ μm all metals exhibit the relation

$$\varepsilon(T, \Omega) \propto T \quad @ \text{ metals}$$

and therefore

$$M = \varepsilon(T, \Omega) \cdot \sigma T^4 \propto T^5 \quad @ \text{ metals}$$

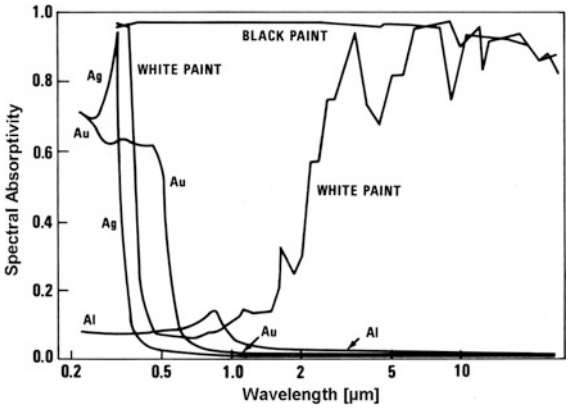

Fig. 16.3 Wavelength-dependent absorptivity of some spectrally selective surfaces. *Credit* NASA

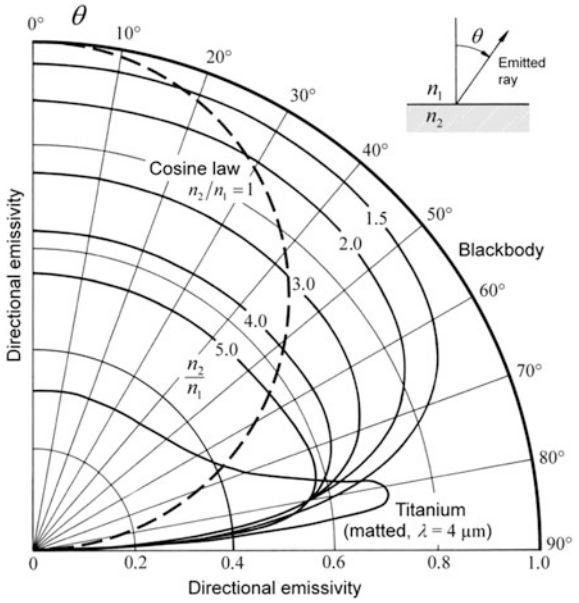

Fig. 16.4 Directional emissivity of selective plane surfaces: dielectric materials with $n_2/n_1 > 1$, matted titanium as an example of metals, compared to Lambert's cosine law, and a diffuse black-body radiator

Because with increasing/decreasing brightness temperature T the spectral exitance shifts towards lower/higher wavelengths via Wien's displacement law Eq. (16.1.20) this implies that for metals ε_λ strongly increases with decreasing wavelength, typically by a factor of 3 (iron, platinum, nickel, titanium) in the range $\lambda = 1{-}10$ μm. This is why the wavelength is given for the emissivity of matted

titanium in Fig. 16.4. A notable exception from this rule is copper, with a nearly wavelength- and thus brightness-temperature independent emissivity, thus depending only on directivity and surface properties.

So, Lambert's cosine law is no longer valid for dielectric or metallic surfaces. In the literature, this is quite often overlooked, and metals are treated the same way as diffuse radiators. In practice, this may not make much a difference. In principle, however, it is not admissible and has to be justified in each individual case.

16.1.5 Kirchhoff's Law

We now consider a receiver in radiative equilibrium with its environment. What does "radiative equilibrium" mean? As a matter of fact, every body in our world is exposed to radiation from its environment, and the irradiated body reemits radiation to its environment. We have seen in Sect. 16.1.3 that a body at temperature T has internal energy $k_B T$ and emits heat with the same energy. So, bodies share their internal energy with energies of other bodies by thermal radiation. If radiation is the only means for a body to exchange energy, it is in radiative equilibrium if all received energy equals all emitted energy.

For our theoretical analysis let us assume the simplest case: A radiatively absorbing body is completely surrounded by a black-body radiator. In radiative equilibrium its temperature has to be identical to the temperature T of the black-body radiator. That is, the spectral radiance of its emitted and absorbed radiation must be identical. This conclusion is Kirchhoff's law of thermal radiation:

> *Any body at a given temperature T emits in every solid angle element and in every wavelength interval the same radiative power as it absorbs there from the radiation of a black body having the same temperature.*

In our notation this law reads

$$d^3\Phi_t(T) = \alpha_{\lambda\Omega}(T) \cdot d^3\Phi_\bullet(T) \quad \textbf{Kirchhoff's law}$$

When applying Eq. (16.1.3), this expression translates into

$$L_{\lambda\Omega,t}(T) = \alpha_{\lambda\Omega}(T) L_{\lambda\Omega,\bullet}(T) \tag{16.1.32}$$

It tells us that the spectral radiance $L_{\lambda\Omega}$ of any radiating body in radiative equilibrium with its environment can be traced back to the spectral radiance of a black body. This is the significance of Kirchhoff's law.

$\alpha = \varepsilon$ Identities

When applying Eq. (16.1.23), $L_{\lambda\Omega,t} = \varepsilon_{\lambda\Omega}(T) L_{\lambda\Omega,\bullet}$, we get an alternative formulation of Kirchhoff's law

$$\alpha_{\lambda\Omega}(T) = \varepsilon_{\lambda\Omega}(T) \quad @ \quad T_t = T_r =: T \tag{16.1.33}$$

So, as long as a body is in radiative equilibrium with any environment, Eq. (16.1.33) is always valid.

We now want to find similar identities as Eq. (16.1.33) for the directional total emissivity/absorptivity and the hemispherical total emissivity/absorptivity.

From Eqs. (16.1.27) to (16.1.29) we get the identity

$$\varepsilon_\Omega(T) = \frac{\left[\varepsilon_{\lambda\Omega} L_{\lambda\Omega,\bullet}\right]_\lambda}{L_{\Omega,\bullet}} \overset{!}{=} \frac{\left[\alpha_{\lambda\Omega} L_{\lambda\Omega,r}\right]_\lambda}{\left[L_{\lambda\Omega,r}\right]_\lambda} = \alpha_\Omega(T)$$

This inner equation holds, if

- $\left[\varepsilon_{\lambda\Omega} L_{\lambda\Omega,\bullet}\right]_\lambda = \varepsilon_{\lambda\Omega}\left[L_{\lambda\Omega,\bullet}\right]_\lambda = \varepsilon_{\lambda\Omega} L_{\Omega,\bullet}$ plus $\left[\alpha_{\lambda\Omega} L_{\lambda\Omega,r}\right]_\lambda = \alpha_{\lambda\Omega}\left[L_{\lambda\Omega,r}\right]_\lambda$, or
- $L_{\lambda\Omega,r}(\lambda) \propto L_{\lambda\Omega,\bullet}(\lambda)$, i.e. if the incident radiation has a spectral distribution proportional to that of a black body at T. In other words:

$$\varepsilon_\Omega(T) = \alpha_\Omega(T) \quad @ \quad T_t = T_r =: T \tag{16.1.34}$$

holds if

- $\varepsilon_{\lambda\Omega} = \alpha_{\lambda\Omega}$ is independent of the wavelength, or
- The incident radiation has a spectral distribution proportional to that of a black body at T.

From Eqs. (16.1.27) to (16.1.29) we get the identity

$$\varepsilon(T) = \frac{\left[\varepsilon_\Omega \cos\theta_t\right]_\Omega}{\pi} \overset{!}{=} \frac{\left[\alpha_\Omega L_{\Omega,r} \cos\theta_r\right]_\Omega}{\left[L_{\Omega,r} \cos\theta_r\right]_\Omega} = \alpha(T)$$

The inner equation holds only if $\varepsilon_\Omega(T) = \alpha_\Omega(T)$ and if

- $\varepsilon_\Omega, \alpha_\Omega$ are and hence $\varepsilon_{\lambda\Omega} = \alpha_{\lambda\Omega}$ is independent of angle, or
- $L_{\Omega,r}(\not{\Omega})$, i.e. the incident radiation is independent of incident angle, i.e. it is diffuse.

This implies:

$$\varepsilon(T) = \alpha(T) \quad @ \quad T_t = T_r =: T \tag{16.1.35}$$

which holds if

- $\varepsilon_{\lambda\Omega} = \alpha_{\lambda\Omega}$ is independent of wavelength and angle (= gray body); or
- the incident radiation is diffuse and has a spectral distribution proportional to that of a black body at T (= gray environment); or
- $\varepsilon_{\lambda\Omega} = \alpha_{\lambda\Omega}$ is independent of angle plus the incident radiation has a spectral distribution proportional to that of a black body at T.

Note, from the above derivation it also follows that if the spectral temperatures of the incident and emanating radiation are NOT the same, i.e. $T_t \neq T_r$, then

$$\boxed{\alpha(T_t) \neq \varepsilon(T_r)} \quad @ \quad T_t \neq T_r \tag{16.1.36}$$

Usually, this is the case for a body in an extreme environment, such as a spacecraft in space receiving solar radiation with radiation temperature $T_{sol} \approx 5778$ K and emitting into deep space that has a radiation temperature $T_{space} = 2.73$ K.

Gray-Body Radiator

The problem of determining radiation exchange between surfaces within a spacecraft, as approached in Sect. 16.2, is greatly simplified if Eq. (16.1.35) holds for a given surface. One of the conditions for Eq. (16.1.35) reads "$\varepsilon_{\lambda\Omega} = \alpha_{\lambda\Omega}$ is independent of wavelength and angle", In other words, a surface that inherits all the properties of a black-body radiator, except that it radiates with a spectrally and directionally constant fraction of the black-body radiator exhibits the property

$$\varepsilon(T) = \alpha(T) < 1 \quad @ \quad \text{gray body} \tag{16.1.37}$$

Such bodies are called *gray bodies* or *gray surfaces*. In particular they radiate diffusively and hence are diffuse surfaces. Therefore they sometimes are also called *diffuse-gray surfaces.*

16.2 Radiation Exchange

Now that we know the emission and absorption characteristics of different surfaces, especially those of diffuse surfaces, we want to know how much radiation energy is exchanged between two surfaces.

16.2.1 Transmitted and Absorbed Flux

Let us have a closer look at a radiating surface dA_t that transmits radiant flux to a receiver surface dA_r, each of both having orientation θ_t and θ_r between their surface normal and the interconnecting ray line. According to Eq. (16.1.11), this transmitted flux can be written as

$$d^2\Phi_{t\to r} = L_{\Omega,t} \cdot dA_{t,\perp} d\Omega_r = \frac{1}{s^2} L_{\Omega,t} \cdot dA_{\perp,t} dA_{\perp,r} \tag{16.2.1}$$

where s is the distance from the transmitter to the receiver and the latter follows from the definition of the solid angle (see Fig. 16.1)

$$s^2 \cdot d\Omega_r = dA_{\perp,r} = \cos\theta_r \cdot dA_r$$

In summary, we get

$$d^2\Phi_{t\to r} = \frac{1}{s^2} L_{\Omega,t} \cos\theta_t \cos\theta_r \cdot dA_r dA_t \tag{16.2.2}$$

This radiant flux in *Watt* units describes the transmission of photons per unit time emitted from the transmitter in direction Ω to the receiver at distance s.

Absorbed Radiant Flux
The emitted radiant flux will somewhere hit a receiving surface, which absorbs at least a fraction of it. To determine the absorbed radiant flux let us assume that the transmitter is a diffuse (Lambertian) radiator as described in Sect. 16.1.2, which, on average over all radiators, is a good assumption. According to Eqs. (16.1.31), (16.2.2), and (16.1.16b) we then have

$$d^2\Phi_a = \alpha_r \cdot d^2\Phi_{t\to r} = \alpha_r \frac{M}{\pi s^2} \cos\theta_t \cos\theta_r \cdot dA_r dA_t \tag{16.2.3}$$

Remark *For physical correctness, in the above we should have written* $s^2 \cdot d\Omega_r = \cos\theta_r \cdot dA_r \cdot 1[sr]$ *and* Eq. (16.2.2) *therefore should read* $d^2\Phi_{t\to r} = L_{\Omega,t} \cos\theta_t \cos\theta_r / s^2 \cdot dA_r dA_t \cdot 1[sr]$. *However, since in* Eq. (16.2.3) π *is in units* $[sr]$ (*see comment after* Eq. (16.1.16b)), *the unit* $[sr]$ *cancels out. So, from now on* π *is dimensionless.*

The total radiant flux between emitter surface A_t and absorber surface A_r is the double integral over both sides of this equation. By carrying out this operation and with Eq. (16.1.26) the absorbed radiant flux at the receiver becomes

$$\boxed{\Phi_a = \alpha_r \varepsilon_t A_t F_{t\to r} \sigma T_t^4} \tag{16.2.4}$$

where $F_{t\to r}$ is the so-called *view factor* as discussed in the next section. We recall that the receiver absorbs the transmitted spectrum and hence $\alpha_r(T_t)$.

16.2.2 View Factor

In Eq. (16.2.4) we have introduced the dimensionless *view factor* (a.k.a. *configuration factor, shape factor, angle factor, or exchange factor*)

$$F_{t\to r} := \frac{1}{A_t} \int_{A_r} \int_{A_t} \frac{\cos\theta_t \cos\theta_r}{\pi s^2} \cdot dA_t dA_r \le 1 \quad \textbf{view factor} \tag{16.2.5}$$

A_t, A_r transmitter surface or receiver surface respectively
θ_t, θ_r angle between radiation line and the surface normal
s distance between the two surface points.

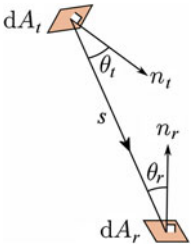

The view factor is the proportion of radiation emitted from A_t that reaches A_r. So

$$F_{t\to r} = \frac{\Phi_{t\to r}}{\Phi_t} = \frac{\Phi_{t\to r}}{M_L(T_t)A_t}$$

The view factor describes the vision geometry between transmitter and receiver surfaces: What does surface A_r see of surface A_t? By definition, the view factor is non-dimensional and smaller than or equal 1. The following three properties hold for the view factor: Since the sum of all surfaces A_r that are external with regard to the transmitter have to fill the total visible solid angle, the emitted radiation will hit any surface around the transmitter. Therefore, the following rule must be valid

$$\sum_{all\ r} F_{t\to r} = 1 \quad \textbf{summation rule} \tag{16.2.6}$$

Second, because of the commutability of the integration variables in Eq. (16.2.5), we directly get

$$A_t F_{t\to r} = A_r F_{r\to t} \quad \textbf{reciprocity relation} \tag{16.2.7}$$

Thirdly, because for the total absorbed radiant flux between two emitters 1, 2 and two absorber surfaces 3, 4 the following has to be valid

$$\Phi_{a,1+2\to 3+4} = \Phi_{a,1\to 3} + \Phi_{a,1\to 4} + \Phi_{a,2\to 3} + \Phi_{a,2\to 4}$$

This results with Eq. (16.2.4) in the so called *addition theorem*

$$\begin{aligned}(A_1 + A_2)F_{1+2\to 3+4} = {} & A_1F_{1\to 3} + A_1F_{1\to 4} \\ & + A_2F_{2\to 3} + A_2F_{2\to 4} \quad \textbf{addition theorem}\end{aligned} \tag{16.2.8}$$

Compilation of View Factors

It is quite easy to calculate the visual factor for two flat plates at a distance of s, and with $A_t, A_r \ll \pi s^2$. In this case, the angles θ_t, θ_r are more or less constant along the integration area. So we get

$$F_{plate\ A_t \rightarrow plate\ A_r} = \cos\theta_t \cos\theta_r \frac{A_t}{\pi s^2} \tag{16.2.9}$$

If a spacecraft is considered a plate or a small sphere we can also get relatively simple expressions for the view factors for a spacecraft circling a spherical celestial body (planet)

$$F_{plate \rightarrow sphere} = \mu^2 \cos\phi \quad \text{for} \quad \phi + \arcsin\mu < \frac{\pi}{2} \tag{16.2.10}$$

$$F_{small\ sphere \rightarrow big\ sphere} = \frac{1}{2}\left(1 - \sqrt{1-\mu^2}\right) \tag{16.2.11}$$

with

$$\mu = R/(R+h)$$

- h orbit altitude above the surface of the planet
- R radius of the planet
- ϕ angle between the orbital position vector and the surface normal of the S/C.

Compilations of these and many different geometries can be found on Howell's website www.thermalradiation.net/tablecon.html.

Multiple Reflection

For thermal radiation between two surfaces we also have to consider multiple reflection as well as the mutual proximity of the surfaces. This is taken into account by the *form factor* $\Im_{i \leftrightarrow j}$. Hence, the form factor for two parallel plates with infinite extent and the emission parameters ε_i and ε_j is no longer (see Eq. (16.2.9)) $F_{i \rightarrow j} = F_{j \rightarrow i} = 1$, but (see Howell 2011)

$$\Im_{i \leftrightarrow j} = \frac{1}{1/\varepsilon_i + 1/\varepsilon_j - 1} \tag{16.2.12}$$

If even the surface i is able to see itself (concave curvature) the following is valid

$$\Im_{i \leftrightarrow (i,j)} = \frac{F_{i \rightarrow i}}{1/\varepsilon_i + (1 - F_{i \rightarrow i})(1/\varepsilon_j - 1)} \tag{16.2.13}$$

This shows how complicated such calculations may become.

If surfaces become arbitrarily complex, the only way to handle this problem is to use the so-called ***ray tracing process***. Hereby, rays are generated by Monte Carlo statistics and the path of each individual ray is traced between given surfaces with

their given emissivities and absorptivities. These ray tracing tools are highly complicated, but also highly accurate (see Subsection *Monte Carlo Ray Tracing* in Sect. 16.3.4).

16.2.3 Point Radiators

Point radiators, such as the Sun, are specific for compiling the absorbed radiant flux as given in Eq. (16.2.4). On one hand, owing to a high surface temperature their radiant exitance is extremely large. Yet, due to the large distance only a very small amount of this radiation hits a receiver on a distant planet, implying that the view factor is very small. So we need to investigate the expression $A_t F_{t\to r}\sigma T_t^4$.

Let us assume the point-like radiator has a circular effective (projected) transmitter surface $A_{t,\perp} = \pi R_t^2$. Because the source appears to be a point, it must be very far away, i.e. $s \gg R_t$. Thus and applying Eq. (16.1.17) we can simplify the view factor Eq. (16.2.5) as

$$\begin{aligned} A_t F_{t\to r} &= \int_{A_r}\int_{A_t} \frac{\cos\theta_t \cos\theta_r}{\pi s^2}\cdot dA_t dA_r = \frac{1}{\pi s^2}\int_{A_r}\int_{A_t} \cos\theta_t \cos\theta_r \cdot dA_t dA_r \\ &= \int_{A_r} \cos\theta_t \cdot dA_t \times \int_{A_t} \cos\theta_r \cdot dA_r = \frac{1}{\pi s^2} A_{t,\perp} A_{r,\perp} = \left(\frac{R_t}{s^2}\right)^2 A_{r,\perp} \end{aligned}$$

For the absorbed radiant flux Eq. (16.2.4) we hence obtain

$$\Phi_a = \alpha_r \varepsilon_t A_t F_{t\to r}\sigma T_t^4 = \alpha_r \varepsilon_t \sigma T_t^4 \left(\frac{R_t}{s}\right)^2 A_{r,\perp}$$

With the definition

$$T_{t,eff} := T_t\sqrt{R_t/s} \quad \textbf{effective temperature} \tag{16.2.14}$$

we finally get

$$\Phi_a = \alpha_r(T_t)\varepsilon_t A_{r\perp}\sigma T_{t,eff}^4 \tag{16.2.15}$$

This expression for the radiant flux is obviously more practical than Eq. (16.2.4). A comparison of Eq. (16.2.4) with Eq. (16.2.15) reveals that the introduction of the effective temperature accomplishes the following formal substitution

$$A_t F_{t\to r} T_t^4 \to A_{r\perp} T_{t,eff}^4 \tag{16.2.16}$$

Note *The effective temperature merely simplifies the computation of the radiant flux onto a receiver. However, the radiation temperature is still the temperature of the actual radiating surface. In the case of the Sun it is* $T_{sun} = 5778$ K *and the absorptivity of received solar radiation is thus* $\alpha_r(5778\ \mathrm{K})$.

Sun as a Point Radiator

The Sun is an excellent example of a point radiator (black-body radiator). It has $T_{sun} = 5778$ K, an apparent $R_{sun} = 695{,}000$ km, and mean distance $s = 1.496 \times 10^8$ km to Earth. The effective temperature for a solar irradiation perpendicular to a surface at the Earth's distance therefore is

$$T_{sun,eff} = 5778\ \mathrm{K}\sqrt{\frac{0.6959}{149.6}} = 394.4\ \mathrm{K} \tag{16.2.17}$$

Let us do a quick cross check to make sure the result is correct. The seasonal irradiation of Earth by the Sun is given by

$$E_{sun\to earth\perp} = S_0 \cdot \left[1 + 0.034 \cdot \cos\left(360^\circ \frac{n}{365}\right)\right] \frac{W}{m^2} = 1361.5 \pm 46 \frac{W}{m^2}$$

where $S_0 = 1361.5\ W/m^2$ is the solar constant (mean irradiation) and n = day of the year (January 1: $n = 1$). For the effective temperature of the Sun this results in

$$T_{sun,eff} = \left(\frac{E_{sun\to earth\perp}}{\sigma}\right)^{1/4} = \left(\frac{1361.5 \pm 46}{5.6704 \times 10^{-8}}\ \mathrm{K}^4\right)^{1/4} = 394 \pm 3\ \mathrm{K}$$

16.2.4 Radiation Exchange Between Two Bodies

We are now prepared to derive the expression for an effective radiant flux exchange Φ_{ij} between two surfaces i and j. According to Eq. (16.2.4) we get

$$\Phi_{i\to j} = \alpha_j(T_i)\varepsilon_i(T_i)A_iF_{i\to j}\sigma T_i^4 - \alpha_i(T_j)\varepsilon_j(T_j)A_jF_{j\to i}\sigma T_j^4$$

From Eq. (16.2.7) we have $A_iF_{i\to j} = A_jF_{j\to i}$ and therefore

$$\Phi_{i\to j} = A_iF_{i\to j}\sigma\left[\alpha_j(T_i)\varepsilon_i(T_i)T_i^4 - \alpha_i(T_j)\varepsilon_j(T_j)T_j^4\right] \tag{16.2.18}$$

If for the transmitter and receiver surfaces $\alpha_j(T_i)\varepsilon_i(T_i) \approx \alpha_i(T_j)\varepsilon_j(T_j)$, we finally get for the effective radiant flux $i \to j$

$$\boxed{\Phi_{i\to j} = \varepsilon_i \alpha_j A_i F_{i\to j} \sigma\left(T_i^4 - T_j^4\right)} \quad @ \quad \alpha_j(T_i)\varepsilon_i(T_i) \approx \alpha_i\left(T_j\right)\varepsilon_j\left(T_j\right) \tag{16.2.19}$$

The condition holds in particular if $\alpha_j(T_i) \approx \varepsilon_j\left(T_j\right)$ plus $\alpha_i\left(T_j\right) \approx \varepsilon_i(T_i)$, which according to Eq. (16.1.35) is the case

- if $T_i \approx T_j$, or
- for black bodies with $\alpha = \varepsilon = 1$, or
- for gray surfaces having $\alpha = \varepsilon = const < 1$,

Multiple Reflection Between Large Parallel Flat Plates

In the case where we have two large parallel flat plates, both of size A, but different emissivities ε_i, ε_j, with multiple reflections between them, we have seen from Eq. (16.2.12) that we have to consider the form factor $\Im_{i\leftrightarrow j}$. Since a ray between these two plates will be absorbed eventually it seems conclusive (see Howell 2011) that

$$\varepsilon_i \alpha_j F_{i\to j} \to \frac{1}{1/\varepsilon_i(T_i) + 1/\varepsilon_j\left(T_j\right) - 1}$$

and therefore

$$\boxed{\Phi_{i\to j} = \frac{A\sigma\left(T_i^4 - T_j^4\right)}{1/\varepsilon_i(T_i) + 1/\varepsilon_j\left(T_j\right) - 1}} \quad @ \text{ large parallel flat plates} \tag{16.2.20}$$

Case in Point: Multi-Layer Insulation

We want to explore the effect of shielding layers on insulation properties as exploited by so-called multi-layer insulation blankets. MLI blankets are extensively used in spacecraft as lightweight thermal protection systems. An example for a commonly used outer layer is a 25–50 μm Kapton film (which give the MLI its typical gold color) backed with a few Angstrom thick layer of vapor deposited aluminum (VDA), The multiple layers in the blanket are usually 6 μm Mylar (or Kapton) with a few Angstrom thick layer of VDA on each side, which makes them look like aluminum foil. The layers are separated by a spacer netting ("bridal veil") or felt-like structure, made for example from dacron, which prevents contact of the adjacent foils (see Fig. 16.5). Heat transfer analysis has shown that the radiant flux at room temperature dominates the conductive flux through a MLI blanket by about one order of magnitude. We will therefore focus here on the radiative insulation property of shielding layers.

We assume that a body with a flat surface and a given temperature T_0 exchanges radiation with a "flat" external environment having effective temperature T_∞. According to Eq. (16.2.20) the radiant exitance to the external environment then is

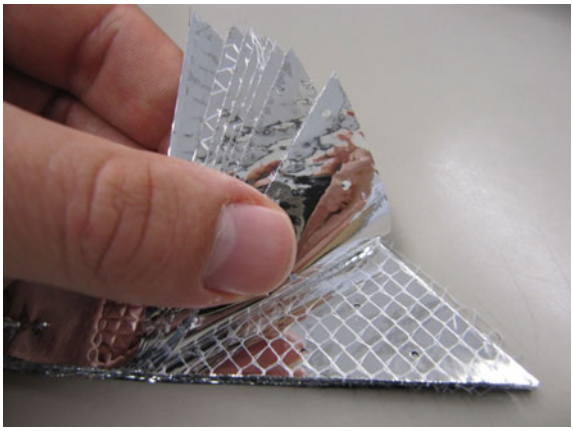

Fig. 16.5 A typical MLI blanket with VDA Kapton layers and dacron netting in between. *Credit* IRS/Uni Stuttgart

$$\Phi_{0\to\infty} = \frac{A\sigma\left(T_0^4 - T_\infty^4\right)}{1/\varepsilon_0 - 1/\varepsilon_\infty - 1}$$

We now add n thermal shielding layers between the body and its environment and assume that both sides of the layers have the same emissivity ε. Since the radiant exitance (heat flow), $M = \Phi/A$, has to be identical from layer to layer we therefore get the following set of $n + 1$ equations

$$\begin{gathered} M(1/\varepsilon_0 + 1/\varepsilon - 1) = \sigma\left(T_0^4 - T_1^4\right) \\ M(2/\varepsilon - 1) = \sigma\left(T_1^4 - T_2^4\right) \\ \cdots \\ M(2/\varepsilon - 1) = \sigma\left(T_i^4 - T_j^4\right) \\ \cdots \\ M(1/\varepsilon + 1/\varepsilon_\infty - 1) = \sigma\left(T_n^4 - T_\infty^4\right) \end{gathered}$$

Adding all these equations each side by itself results in

$$M\left[\frac{1}{\varepsilon_0} + \frac{1}{\varepsilon_\infty} - 1 + n\left(\frac{2}{\varepsilon} - 1\right)\right] = \sigma\left(T_0^4 - T_\infty^4\right)$$

Typically $\varepsilon_0 \approx \varepsilon_\infty \approx 0.8$, while an MLI has tens of layers with $\varepsilon \approx 0.068$. So, we do not make a big error if we neglect the $\varepsilon_0, \varepsilon_\infty$ terms. Hence we finally find

$$\Phi_{n\to\infty} = \frac{\Phi_{0\to\infty}}{1/\varepsilon_0 + 1/\varepsilon_\infty - 1 + n(2/\varepsilon - 1)} \approx \frac{\Phi_{0\to\infty}}{n(2/\varepsilon - 1)} \quad @\ n \text{ shielding layers} \tag{16.2.21}$$

where $\Phi_{0\to\infty}$ was the unshielded radiant flux. Verbalized:

> A multi-layer insulation with n shielding layers reduces the effective radiant flux between a given body and its environment typically by a factor of $0.035/n$.

Example

Assume we have a deep space probe shielded by MLI with the internal MLI layer of $T_0 = 300$ K and the outer layer (facing deep space) at a temperature of $T_0 \approx 150$ K. Then, with a 30 layer MLI we have an emitted radiant exitance

$$M_{rad} \approx \frac{0.035}{30}\sigma\left(300\text{K}^4 - 150\text{K}^4\right) = 0.50\ \frac{\text{W}}{\text{m}^2}$$

For comparison, the conduction heat transfer (cf. Eq. (16.3.3)) through the layers, $M_{n\to\infty} = G(T_0 - T_\infty)$, is measured to be very roughly $G \approx 5 \times 10^{-3}$ W m^{-2} K^{-1}. Therefore

$$M_{cond} \approx 0.005\ \frac{\text{W}}{\text{m}^2\ \text{K}} \cdot (300\ \text{K} - 150\ \text{K}) = 0.75\ \frac{\text{W}}{\text{m}^2}$$

In this example, at these temperatures (inner layer 300 K, outer layer 150 K), the conduction heat transfer would be of about the same magnitude as the radiation heat transfer, and hence well-balanced.
In reality, both the total heat transfer and the share between conduction and radiation heat transfer through MLI is temperature dependent. Generally, the radiative heat transfer gains significance with increasing temperature and vice versa. If, for example, the outer layer is not 150 K but 450 K due to the exposure to the Sun the radiative share is $M_{rad} = -2.18$ W/m^2 and the conductive $M_{cond} = -0.75$ W/m^2, i.e. no longer well-balanced. Therefore, in practical applications the heat transfer through an MLI must be generally considered as a function of the MLI's temperature.
In addition, the efficiency of MLI layers and the share between radiative and conductive heat transfer also vary with the number of layers, layup type, and even from layup to layup due to different workmanship.

16.2.5 Spacecraft Thermal Balance

We now consider an arbitrary body B without internal radiation source exchanging radiation with many surrounding bodies $1, 2, 3, \ldots$ all having different temperatures. Therefore and in contrast to Eq. (16.1.35) we have $\alpha_B(T_i) \neq \varepsilon_B(T_j)$ and $\alpha_B(T_i) \neq \alpha_B(T_j)$. Because the radiation of the different radiation sources is not

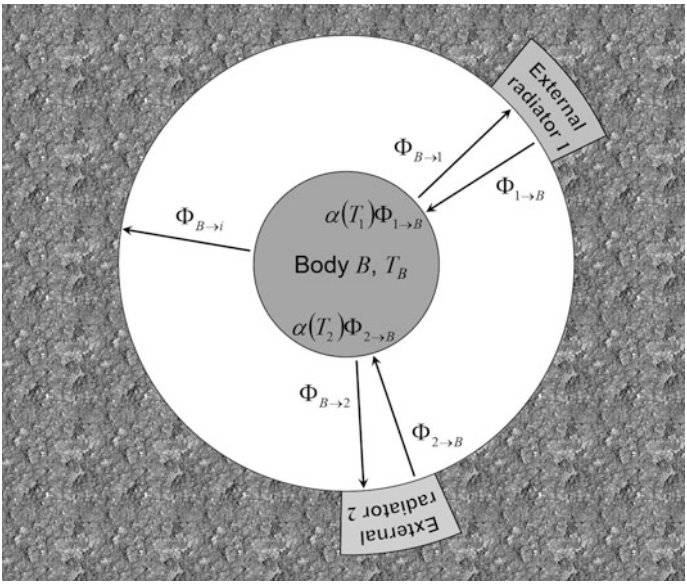

Fig. 16.6 Radiation balance between a body B and its environment with two representative external radiators

necessarily diffuse (see Fig. 16.6), we have to take into account the radiant flux balance with the radiators involved. First, there is the radiant flux emitted by the body B. According to Eqs. (16.1.5) and (16.1.21), it is

$$\Phi_B = M_B(T_B) \cdot A_B = \varepsilon_B A_B \sigma \, T_B^4 \tag{16.2.22}$$

On the other hand, there is the incoming radiation of the surrounding bodies i. With Eqs. (16.2.4) and (16.2.7) it can be written as

$$\begin{aligned} \Phi_a &= \sum_i \alpha_B(T_i) \cdot \Phi_{i\to B} = \sum_i \alpha_B(T_i) A_i F_{i\to B} \varepsilon_i(T_i) \sigma T_i^4 \\ &= A_B \sum_i \alpha_B(T_i) F_{B\to i} \varepsilon_i(T_i) \sigma T_i^4 \end{aligned} \tag{16.2.23}$$

Equating Eq. (16.2.22) with Eq. (16.2.23) results in

$$\varepsilon_B T_B^4 = \sum_i \alpha_B(T_i) \varepsilon_i(T_i) F_{B\to i} T_i^4 + \frac{\Phi_{\text{int}}}{A_B \sigma} \quad \textbf{radiative equilibrium law} \tag{16.2.24}$$

where we now consider also an internal source with heat flux Φ_{int}.

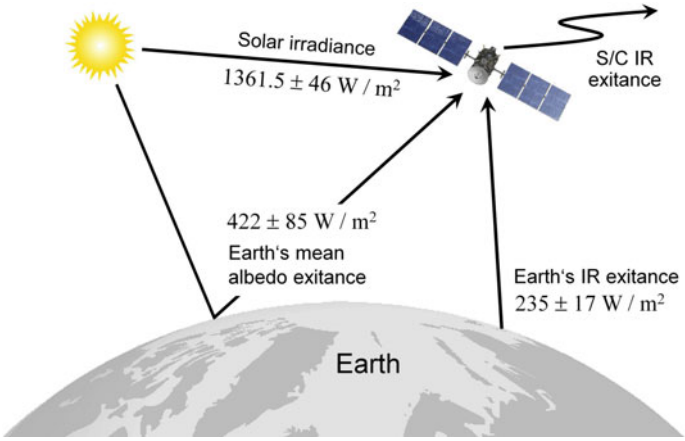

Fig. 16.7 Radiation balance of a satellite in Earth orbit

With Eq. (16.2.24) we are able to set up a thermal balance equation for any spacecraft in space as depicted in Fig. 16.7 and to calculate from it the wanted equilibrium body temperature T_B.

Here we assume a satellite (sat) in Earth orbit exchanging radiation with the Sun, Earth, and space. It is a valid assumption that each of the three bodies radiates like a black-body $(\varepsilon_i = 1)$. Applying this to Eq. (16.2.23), and applying the effective temperature concept, Eq. (16.2.16), to the Sun as a point-source we get

$$\begin{aligned}\varepsilon_{IR} T_{sat}^4 = {} & \alpha_{sol}\delta_{sun}\frac{A_{sat\perp sun}}{A_{sat}} T_{sun,eff}^4 + \alpha_{sol}\delta_a(\gamma) F_{sat\to earth} a T_{sun,eff}^4 \\ & + \alpha_{IR} F_{sat\to earth} T_{earth}^4 + \alpha_{IR} F_{sat\to\infty} T_\infty^4 + \frac{\Phi_{\text{int}}}{A_{sat}\sigma}\end{aligned} \tag{16.2.25}$$

The first term on the right side of the equation corresponds to the absorbed solar radiation, the second term to the absorbed albedo from the Earth, the third term to the absorbed thermal radiation from the Earth, the fourth term to the absorbed radiation from the depths of space, and the last term to the heat generated by the satellite itself.

The given quantities take on the following values:

T_{sat} Temperature of the satellite (or any S/C).

T_{earth} Mean radiation temperature of the Earth = 254 K. This corresponds to an IR radiant exitance at Earth's surface of $0.25(1-a)\cdot 1361.5\ \text{W m}^{-2} = 235 \pm 17\ \text{W m}^{-2}$. Note: Terrestrial IR exitance from geothermal heat flow of merely $0.082\ \text{W m}^{-2}$ is negligible compared to the total terrestrial IR exitance.

T_∞ Black-body temperature of space = cosmic background radiation temperature = 2.73 K.

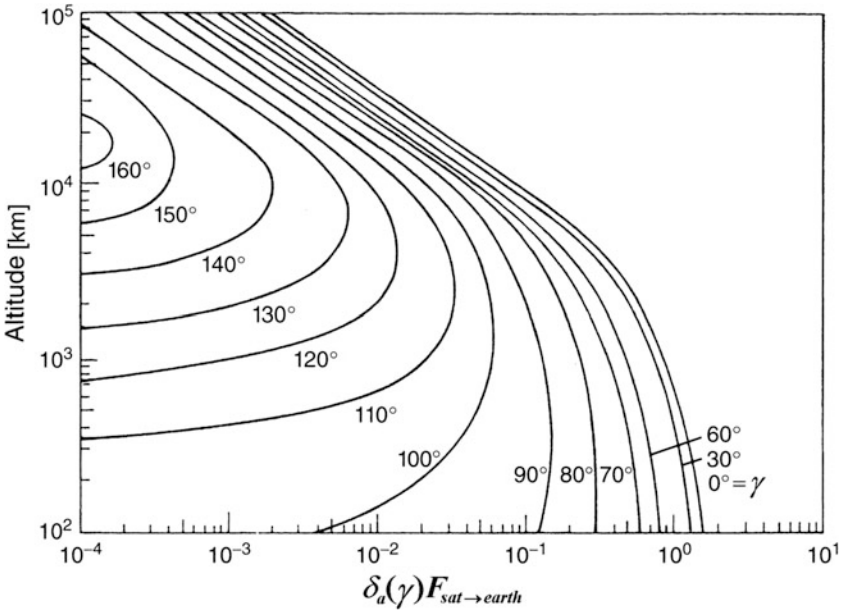

Fig. 16.8 The factor $\delta_a(\gamma)F_{sat\rightarrow earth}$ as a function of orbit altitude and angle γ (see text). *Credit* Fortescue (2003)

$T_{sun,eff}$ Sun's effective temperature at distance 1 AU, $T_{sun,eff} = (394 \pm 3)$ K, where ± 3.3 K is the seasonal change (Jan. 3/July 4).

Φ_{int} Heat flux generated within the satellite (internally).

A_{sat} Total surface of the satellite.

$A_{\text{sat}\perp sun}$ Surface of the spacecraft projected onto the direction to the Sun. The following is valid for a plate (sphere): $A_{sat\perp sun} = 0.5 \cos\theta \cdot A_{sat} (0.25 \cdot A_{sat})$.

α_{sol} $= \alpha_{sat}(T_{sun})$, the absorptivity of the surface of the S/C (see also Eq. (16.1.31) with $T_{sun} = 5762$ K) for solar radiation in the visible spectrum.

ε_{IR} $= \varepsilon_{sat}(T_{sat})$, the infrared emissivity of the surface of the S/C (see Eq. (16.1.26) with T $\approx$ 300 K).

a Albedo of the Earth: a = 0.07 − 0.85, annual average value: 0.31 [0.22 (equator) − 0.69 (south pole)].

δ_{sun} Sun visibility factor. δ_{sun} = 1: Sun shines on satellite. δ_{sun} = 0: Satellite is in the Earth's shadow.

$\delta_a(\gamma)$ Day-side visibility factor, i.e. the day-side proportion of Earth's surface visible at the satellite, $0 \leq \delta_a \leq 1$. It depends on the angle γ, which is the angle between the local vertical (nadir direction) and the direction of the incident solar radiation (not to be confused with Sun's beta angle β, see Sect. 14.1.1). Figure 16.8 depicts the product $\delta_a(\gamma)F_{sat\rightarrow earth}$.

Note *The above values are mean values with regard to space and time, and the error indications only refer to time variations. Spatial variations have not been considered. The latter can be quite considerable for the IR radiation of the Earth (poles!) and for the albedo. The albedo at the subsolar point (when the surface of the Earth is between the geocenter and the Sun) is 0.31 and decreases on either side towards the limb, until it becomes 0.0 at the terminator. This is because albedo represents a reflectivity, and the corresponding thermal flow decreases with the cosine of the radiation angle of the reflected ray. For more precise numerical calculations, one has to consider the beta angle β of the orbit and the current deviation from the subsolar point (see Clawson 2002).*

In the albedo radiation term the Earth always behaves like a black-body radiator with the temperature $T_{sun,eff}$ and an intensity reduced to the albedo. Apart from that, the bright daytime side does not always face the satellite. So the factor δ_a is the relation between the visible part of the daytime surface to the total visible surface of the Earth. As the fourth power of the temperature of space can be neglected with regard to all other temperatures, we finally get

$$T_{sat}^4 = \frac{\alpha_{sol}}{\varepsilon_{IR}} \left(\delta_{sun} \frac{A_{sat\perp sun}}{A_{sat}} T_{sun,eff}^4 + a\delta_a(\gamma) F_{sat\to earth} T_{sun,eff}^4 \right) + F_{sat\to earth} T_{earth}^4 + \frac{\Phi_{\text{int}}}{\varepsilon_{IR} A_{sat} \sigma} \tag{16.2.26}$$

Spherical Satellites Orbiting Earth

Next, we want to derive a simple formula to estimate the S/C temperature near any planet. For that and making the rough (but mostly sound) approximation that a spherical satellite (see Eq. (16.2.11)) is orbiting a planet with radius R at altitude h, then $A_{sat\perp sun} = 0.25 A_{sat}$ holds, and the above thermal balance equation can be reduced to

$$T_{sat}^4 = \frac{\alpha_{sol}}{4\varepsilon_{IR}} (\delta_{sun} + 2a\delta_a F_{sat\to Earth}) T_{sun,eff}^4 + \frac{1}{2} F T_{planet}^4 + \frac{\Phi_{\text{int}}}{\varepsilon_{IR} A_{sat} \sigma} \tag{16.2.27}$$

where

$$F = 1 - \sqrt{1 - \left(\frac{R}{R+h} \right)^2}$$

R radius of the planet

h orbit altitude of the S/C above the surface of the planet.

For a spherical satellite that orbits Earth we specifically get

$$T_{sat} = 279\ \text{K} \cdot \left[\frac{\alpha_{sol}}{\varepsilon_{IR}} (\delta_{sun} + 0.68 \cdot \delta_a F_{sat\to earth}) + 0.328F + \varphi \right]^{1/4} \tag{16.2.28}$$

with

$$\phi = \frac{\Phi_{\text{int}}}{\varepsilon_{IR} A_{sat} \sigma (279\text{K})^4} = \frac{\Phi_{\text{int}}}{\varepsilon_{IR} A_{sat} \cdot 344 \ \left[\text{W/m}^2\right]}$$

Note that Eqs. (16.2.25) to (16.2.28) are just coarse estimates of the actual temperature conditions. If more accurate temperatures are required, numerical modeling and calculations are indispensable, which are usually done jointly with the modeling of the S/C as described in the following sections. Nonetheless, the results so far achieved are a good first guess to obtain an overview of the overall temperature conditions.

16.2.6 α/ε Materials

In the thermal balance equation the factor $\alpha_{sol}/\varepsilon_{IR}$ is the key parameter to control the satellite's temperature. As shown in Fig. 16.9 there exist many materials spanning the range $0.1 \leq \alpha_{sol}/\varepsilon_{IR} \leq 10$. Accordingly, temperature reduction can be easily

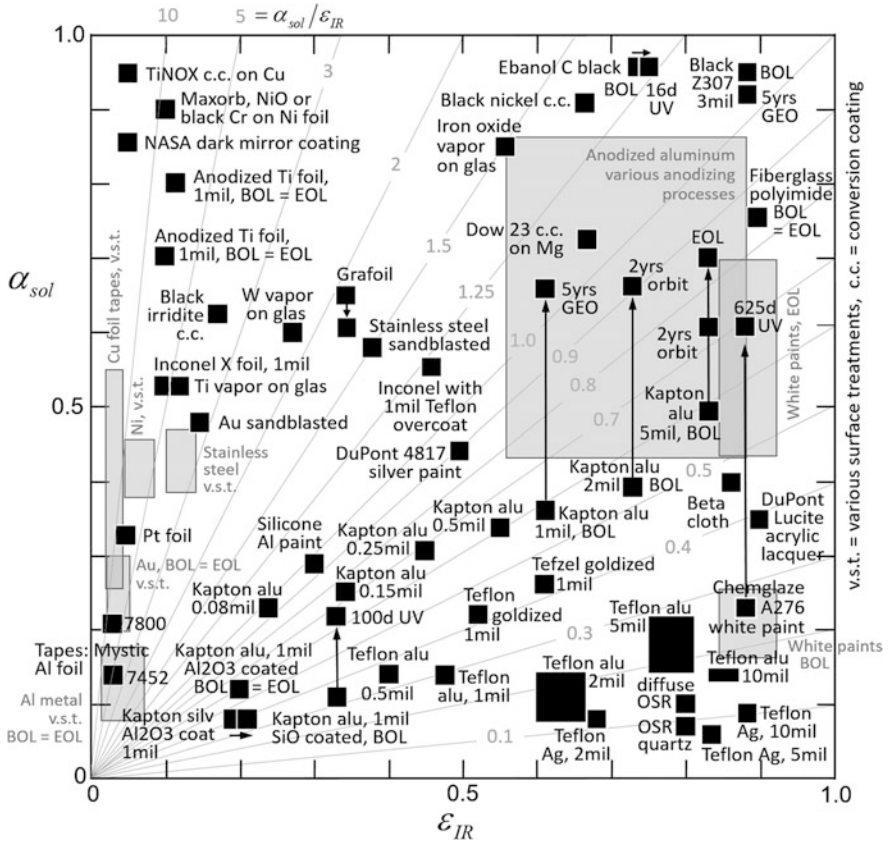

Fig. 16.9 Solar absorption coefficients α_{sol} and infrared emission rates ε_{IR} of different materials. *Data source* Gilmore (2002), Appendix A; © U. Walter

achieved by employing strongly emitting white paint (degrades significantly in space, though) or, even better, so-called **optical solar reflectors** (OSR) or **second surface mirrors** (SSM), namely **silver-coated Teflon** $\alpha_{sol}/\varepsilon_{IR} = 0.12$ or **aluminized Teflon** $\alpha_{sol}/\varepsilon_{IR} = 0.20$. They are made of ultraclear fluorinated ethylene propylene (FEP) Teflon with a thin vapour-deposited layer (0.04–0.4 mm) of silver or aluminum on one side. Silver/Teflon hardly changes under UV radiation, however it degrades rapidly with particle radiation $>10^{15}$ electrons/cm^3 with 5 keV up to 1 meV. SSMs owe their distinct thermal property to the fact that Teflon is a good thermal radiator, whereas the silver coating reflects the incoming sunlight efficiently. As Teflon on the exterior side is relatively inert, the advantage of silver-coated Teflon in relation to other SSMs (such as quartz over silver) is that it hardly degrades.

Outgasing is a special problem of thermal surfaces. Adhesives, elastomers, PC boards, lubricants, and paints as well as the jets of spacecraft reaction control systems generate gases in the vacuum of outer space, which deposit rapidly on surfaces. This can considerably change the absorption and reflection behavior. Apart from that, UV radiation also changes this undesired coating toward larger absorptivity. These impurities are probably the reason for long-term degradation of α/ε material. It can only be corrected by considering the corresponding safety margins.

Atomic Oxygen (AO) is a main cause of surface degradation in LEO. Metals are relatively immune to AO, but other standard thermal materials such as polyester, polyimides and paints are very sensitive to AO.

Electric Charging may occur at higher altitudes. Many thermal materials are excellent insulators, which may lead to sparks and thus damage of the surfaces. Conducting surfaces can remedy the problem. This is another reason why aluminized/ silver-plated Teflon (linked with satellite mass) is a good solution.

Surface Degradation Generally, in thermal design the degradation of the selected coating is a key parameter and a lot of effort is spent by thermal paint developers to characterize the so-called end-of-life (EOL) properties of thermal paints, i.e. their $\alpha_{sol}/\varepsilon_{IR}$ at the end of the spacecraft's life. Sometimes paint samples are sent into space in so-called exposure experiments, to let the paint experience the space environment and to measure the resulting thermo-optical properties after a given exposure time. Other samples can be exposed to accelerated life tests where the samples are exposed to a mix of different radiation sources and atomic oxygen to simulate the aging process.

16.3 Thermal Modeling

P. Hager and M. Czupalla

In Sect. 16.2 the thermal equilibrium and heat exchange between surfaces were derived quite generally from basic physical considerations. From this the heat balance and thus the resulting temperatures of a S/C in space can in principle be derived. This analytical approach provides temperatures of entire bodies or surfaces in thermal equilibrium under a given steady thermal environment.

In reality, the temperatures of a spacecraft are not uniform over its geometry and the thermal environment changes constantly and heavily over an orbit. For instance, a body orbiting a planet is exposed to the Sun on the day-side and not on the night-side. In order to keep critical S/C subsystems within given temperature limits, it is key to determine the temperature distribution of a S/C under such a changing thermal environment.

Pivotal to the determination of these actual S/C temperatures is the thermal modeling process, which on one hand is based upon the above derived analytical considerations, but on the other hand is a quite elaborate process on its own. The purpose of thermal modeling is to verify through a thermal analysis that the designed *thermal control system* (TCS) of a space system meets a set of thermal requirements. The thermal control system is the entirety of thermal control hardware and concepts to control S/C temperatures, temperature gradients and temperature stability.

Based on the results of Sect. 16.2, we introduce in this section the thermal modeling process as implemented in today's thermal design tools for space applications. The approach is as follows. In the first Sect. 16.3.1 we outline the typical requirements for a thermal control system that must be achieved by the thermal design, along with the boundary conditions limiting the solution space.

The subsequent Sect. 16.3.2 extends the simple analytical approach derived for an overall spacecraft heat balance to a series of heat balance equations capable of capturing spatial and temporal temperature gradients. This section is the starting point for the numerical approach behind thermal models.

Next, Sect. 16.3.3 explains how thermal models are set up and how a space system is partitioned into multiple nodes, each having its own heat equation with specific boundary conditions.

The two core parts of a thermal model, the so-called *Geometrical Mathematical Model* and the *Thermal Mathematical Model*, are introduced in two Sects. 16.3.4 and 16.3.5 thereafter.

In Sect. 16.3.6, we show how thermal models are applied in a thermal analysis process, in order to fully validate the thermal design.

The last Sect. 16.3.7 demonstrates by some simple case studies how thermal mathematical models are set up and analyzed.

16.3.1 Thermal Requirements and Boundary Conditions

To assure a specified thermal behavior of a S/C, the thermal modeling of a S/C in its entirety and its thermal environment are required. Thermal requirements in turn are derived from functional and/or performance requirements. The key requirements for thermal analysis are the temperature limits of the individual components, spatial temperature gradients, and temporal temperature gradients. Temporal temperature gradients are more commonly referred to as *temperature stability*. Temperature limits are distinguished into operational and non-operational temperature limits and applied if recurring or 'off-the-shelf' components are used. A typical example for recurring components with a narrow temperature range are batteries. For batteries, particularly Li-ion, the operational design temperature-range is approximately −10 to +30 °C while their non-operational temperature design temperature-range approximately is −20 to +60 °C. For new developments or for entire instruments and at the beginning of a project, predefined temperature limits most often do not exist. In such cases, the boundary values are a result of the thermal analysis at higher system levels.

Spatial gradients are specified to forestall thermo-elastic problems, which might lead to functional loss or performance reduction, such as pointing performance reduction of a spaceborne telescope. Typical spatial gradients at the interface between satellite platform and an instrument vary between 3 and 1 °C/m for missions with a high pointing performance requirement. For interfaces between other components of the spacecraft, requirements typically concern interface temperatures and transient conductive as well as radiative heat fluxes.

Temporal gradients chiefly, but not exclusively, impact performance of components, such as optical detectors. An example for a temporal thermal stability requirement is 0.1 °C per orbit. Because thermal stability sometimes is transformed into the frequency domain, it then is specified in units $\mathrm{K}/\sqrt{\mathrm{Hz}}$.

Further requirements to the thermal control system, amongst others, are allocated heater power, mass requirements, or restrictions due to the available volume.

Requirements and boundary conditions are imposed primarily by the environment, in which a space-system is operated (see Sect. 16.2.5), but also by different environments on the ground. For instance, consider a spacecraft that is transported by an aircraft, truck, or ship, sits on the launch pad, or is stored in a clean room. Then it might be exposed at one extreme to tropical and at the other to tundra-like conditions. Although such additional requirements derived from launch campaign activities usually do not drive the S/C thermal design, they need to be taken into account.

Yet other thermal requirements and boundary conditions apply for components being transported in a pressurized vessel to the ISS, along with the then existing convective heat exchange. These peculiarities will not be addressed here.

The thermal requirements and boundary conditions are either verified through thermal analysis, or tests, or a combination thereof. Thermal tests will not be addressed here. For a detailed discussion of tests see for example Gilmore (2002) or

ECSS-ST-E-31C. The verification through thermal analysis is exclusively achieved through the application of thermal modeling.

In summary, the objective of thermal design is the balancing of the incoming and outgoing heat fluxes in a way that keeps the resulting temperatures as well as spatial and temporal temperature gradients in the ranges required to fulfill mission performance. One should keep in mind, though, that the root cause of a temperature problem, is not a given temperature distribution, but the underlying heat fluxes, which must be examined. So, adjustments of the thermal design are achieved by modification of heat fluxes.

16.3.2 Heat Equation

Having sketched the thermal requirements to be verified, we now address the question of how to determine the temperatures inside a spacecraft. The fundamental approach, introduced in Sects. 16.1 and 16.2, allows the computation of heat fluxes and temperatures for simple geometries and steady state conditions on the outside of a spacecraft or for an idealized one-piece-of-spacecraft model (a.k.a. *one-node model*). Yet, the temperatures thus derived are only qualitative and by no means representative of the temperatures of individual components. This is because the temperatures of individual components are also affected by the internal heat dissipation, internal thermal radiation, internal heat convection (convection of gases or liquids), and internal heat conduction (in solid bodies or liquids). Internal temperatures therefore must be calculated by solving the physical heat equation potentially including all these factors

$$\rho c_p \frac{\partial T}{\partial t} = -\nabla \cdot \boldsymbol{\phi} + \phi_{\text{int}}(\boldsymbol{r}, t) \quad \textbf{heat equation} \tag{16.3.1}$$

Here $\boldsymbol{\phi}$ is the 3-dimensional heat flux vector field, i.e. the vector field of heat flow rates per unit area, the term $\phi_{\text{int}}(\boldsymbol{r}, t)$ describes contingent heat flux sources at position $\boldsymbol{r}$ within the S/C, $\nabla = (\partial/\partial x, \partial/\partial y, \partial/\partial z)$ is the nabla operator, ρ is the local mass density, and c_p is the mass-specific heat capacity.

> **Note** *Because the heat equation is a key equation in the physics of transport phenomena, flux here is defined as flow rate per unit area, different from the terminology of flux in radiometry* (*see Note in* Sect. 16.1.1). *This is why here we use the symbol ϕ for flux rather than Φ as in* Sects. 16.1 and 16.2.

Discretized Heat Equation

In view of the upcoming modeling approach we discretize the system subject to heat transfer (here S/C) into small finite elements (a.k.a. *nodes*). The heat equation for a single node i then reads

$$C_i \frac{dT_i}{dt} = \sum_{j \neq i} \Phi_{j \to i} + \Phi_{i,\text{int}} \tag{16.3.2}$$

Here $C_i = c_{p,i}\rho_i V_i$ is the heat capacity of node i, $\Phi_{i,\text{int}}$ is the internally generated heat flux (equals heat flow rate in radiometric terminology), and $\Phi_{j \to i}$ are the radiometric heat fluxes to node i from all other nodes j linked to i.

To solve the node equations for a system we need to determine the $\Phi_{j \to i}$. There are two different types of fluxes with quite different temperature behavior.

Heat Flux by Convection and Conduction

For gas-based heat convection and solid-body-based heat conduction between two point masses at the temperatures T_i and T_j the following linear relation is valid

$$\Phi_{j \to i} = G_{ij}\left(T_j - T_i\right) \tag{16.3.3}$$

with the so-called *coupling coefficient*

$$G_{ij} = \begin{cases} \kappa A_{ij}/l_{ij} & @ \text{ heat conduction} \\ KA_{ij} & @ \text{ heat convection} \end{cases}$$

where

κ heat conduction coefficient
K heat convection coefficient
A_{ij} cross-section area of interface
l_{ij} distance between nodes.

In most thermal analysis software the coupling coefficient is termed *CONDUCTOR* (capital letters denote thermal-model-specific terms).

Radiative Heat Flux

The simple and linear form of Eq. (16.3.3) is not valid for thermal radiation. For that we rather have to resort to Eq. (16.2.19). It reads

$$\Phi_{j \to i} = \alpha_i \varepsilon_j A_j F_{j \to i} \sigma\left(T_j^4 - T_i^4\right) = R_{ij}\sigma\left(T_j^4 - T_i^4\right) \tag{16.3.4}$$

Here the *radiation coupling coefficient* in thermal analysis is defined as

$$R_{ij} = \alpha_i \varepsilon_j A_j F_{j \to i}$$

We recall that Eq. (16.3.4) strictly holds only for $\alpha_j(T_i) \approx \varepsilon_j\left(T_j\right)$ plus $\alpha_i\left(T_j\right) \approx \varepsilon_i(T_i)$. This holds for nodes within a S/C where $T_i \approx T_j$ (see Eq. (16.1.35)) and for heat exchange with external sources (Sun, albedo, Earth IR, space), which in good approximation can be considered as black or gray bodies (see end of Sect. 16.1.5). Therefore, Eq. (16.3.4) can be generally applied in thermal modeling.

Node Equation

Inserting these results for heat convection/conduction and thermal radiation into Eq. (16.3.2) we finally arrive for a single node i at the so-called *node equation*

$$\boxed{C_i \frac{dT_i}{dt} = \sum_{j \neq i} G_{ij}\left(T_j - T_i\right) + \sum_{j \neq i} R_{ij}\sigma\left(T_j^4 - T_i^4\right) + \Phi_i} \quad \textbf{node equation} \qquad (16.3.5)$$

Here Φ_i may now be the sum of node's heat fluxes due to internal heat sources or due to boundary conditions, i.e. heat flows from the environment external to the node.

In conclusion we have established a simple relation for the thermal conductivity Eq. (16.3.3) (linear) and for thermal radiation Eq. (16.3.4), which have to be inserted into the node Eq. (16.3.2). In Sect. 16.3.5 the conductive and radiative coupling coefficient will be addressed in more detail.

Boundary Conditions

In order to solve Eq. (16.3.5), boundary conditions need to be provided, either temperature or heat flux boundary conditions. Mathematically, a temperature is a boundary condition of type 1, i.e. a Dirichlet boundary condition, while heat flux is of type 2, i.e. a Neumann boundary condition. Physically, a temperature boundary (type 1) condition implies a sink (or source) of infinite capacity, as for example the background temperature of deep space or the temperature of a celestial body. A fixed temperature as boundary in a spacecraft has to be treated with care, as it requires a tight control of input power and duty cycle. A heat flux boundary condition for example is a heat flux from the Sun, from Earth, or from any other celestial body. Internally to a spacecraft, a constant heat flux is generated by heaters or by dissipation of electric energy in electronic boxes. Heat fluxes are the prevailing boundary conditions.

The simplified approach expounded above hits its limits already in design phase A of a space mission project. Complex numerical efforts are required to solve a huge set of dependent linear differential equations as given by Eqs. (16.3.3)–(16.3.5) with a given set of boundary conditions. Therefore, a structured mathematical approach of modeling the thermal network in a S/C becomes a necessity. This approach will be addressed in Sects. 16.3.4 and 16.3.5.

16.3.3 Thermal Model Setup

We recall that at a given position $\boldsymbol{r}$ within a given body and time t the heat Eq. (16.3.1) describes the incoming and outgoing heat fluxes (right hand side) and for flux imbalances the resulting temperature changes per time unit (left hand side), whereby the rate values are determined by the local heat capacity. A negative heat imbalance means cooling, while a positive means heating. The heat may enter or leave the body via multiple paths. Hence and independent of the paths, the driver for cooling or heating is the total heat flux.

However, the heat balance equation in its time-invariant form (Eq. 16.2.26) yields only the temperature for the total body at heat balance, that is the average temperature of that entity. Temperature changes and distribution or gradients along any dimension of the body cannot be captured by this approach. The nature of the thermal space environment, however, dictates that the temperature of a satellite cannot be uniform and constant when the Sun illuminates the hull of an orbiting S/C on one side, while the coldness of space acts as a heat sink on the other side. Hence, we are in need of a method that enables us to predict spatially and temporally distributed temperatures as caused by the environment acting via different parts on the S/C.

Model Discretization

The answer to this challenge is a spatial and temporal discretization with the finite difference method. The total S/C is dissected into small and virtually isothermal parts, which can exchange heat with each other and with their environment. The discretized isothermal parts are called *nodes*. A thermal node is defined by the isothermal temperature and the heat capacity (CAPACITANCE) of the part it represents. Nodes do not carry any information about the heat transport properties of the represented part.

The nodes are connected by so-called *CONDUCTORS*, which represent the heat transport capabilities between the two thermal nodes the CONDUCTOR connects. CONDUCTORS can be either conductive, radiative, or convective (not covered here). They are derived from a combination of the heat transport properties of both connected nodes.

In order to manage the network of nodes and CONDUCTORS, a customized Finite Difference Method (FDM) approach is used in space thermal engineering, the so-called *lumped parameter method*. A good introduction to this method is found in Gilmore (2002) and *ESATAN-TMS* (2010). The lumped parameter method has its origin in the analogy to electronic circuits where current flows are modeled by equivalent resistors and capacitors. In the customized FDM approach, nodes and CONDUCTORS have split functionalities and are not necessarily bound to a geometrical representation, though often simulating one. The FDM nodes, representing the heat capacity property CAPACITANCE, describe the transient temperature evolution driven by the heat imbalance, while the CONDUCTORS determine the heat transport network between the nodes and as such drive the spatial temperature distribution. A schematic visualization of the FDM discretization concept used for thermal modeling is shown in Fig. 16.10.

Note that the concept of split functionalities distinguishes the finite difference method (FDM) from the finite element method (FEM), which is used for instance in mechanical engineering. The FEM approach is based on the concept of elements and nodes. Elements are simple finite geometric forms that make up the FEM mesh of the body under consideration. Nodes are the vertices of an element and hold the parameters (deformation, stress, etc.) for the discretized function acting on an element. Being bound to geometry, FEM methods are well suited for conductive problems and quite complicated for radiative ones. In the FDM approach, however,

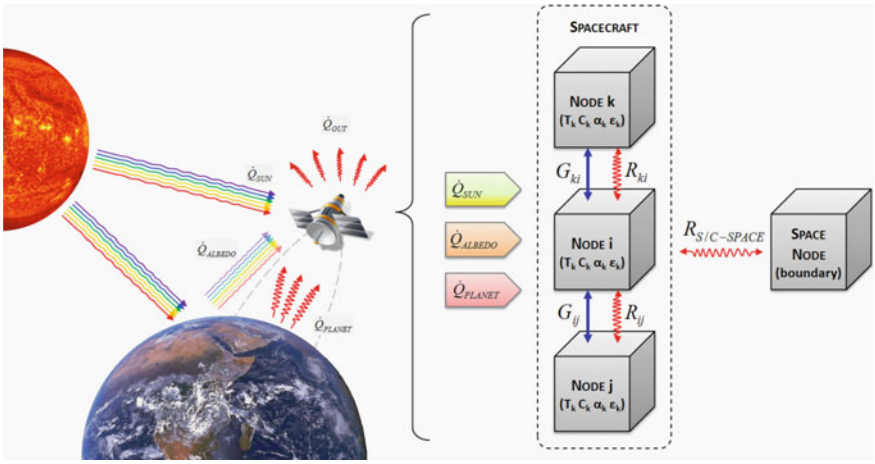

Fig. 16.10 Schematic of the finite differences method applied in S/C thermal modeling

any node can be connected to any other by means of CONDUCTORS. The connection is not geometry dependent which simplifies the modeling of radiative CONDUCTORS.

Thermal Mathematical Model Versus Geometrical Mathematical Model
How is the mesh set up for a specific spacecraft, how are the coupling coefficients (CONDUCTORS) G_{ij} and R_{ij} determined, and how is the discretized heat equation solved? In this paragraph we introduce the setup of thermal models. Thermal models typically consist of a *geometrical mathematical model* (GMM) as pre-processor for the *thermal mathematical model* (TMM). The GMM often comprises also mission specific functionalities for example orbital features that impact heat fluxes or boundary conditions. The logic of this model setup and the connections and interdependencies between the GMM and TMM are explained hereafter and are schematically visualized in Fig. 16.11.

A discretization of a given body or part into nodes yields as many heat equations as there are nodes. The node Eq. (16.3.5) is a first order differential equation. A system with n discretized nodes hence yields n coupled first order differential equations, the solution of which determines the nodal temperatures as enforced by the applied boundary conditions. Such a thermodynamic network with its boundaries is referred to as the *thermal mathematical model* (TMM). It will be discussed in more detail in Sect. 16.3.5. The TMM is the backbone of a thermal analysis.

The TMM can be set up without the need of a geometric model of the system. The discretization can be performed manually, assigning parts of a modeled entity to different nodes and by applying their connections as CONDUCTORS and the necessary boundary conditions in the form of temperatures or heat loads. Particularly for small conductive problems, such as the case study discussed in Sect. 16.3.7 a TMM-only approach may be sufficient.

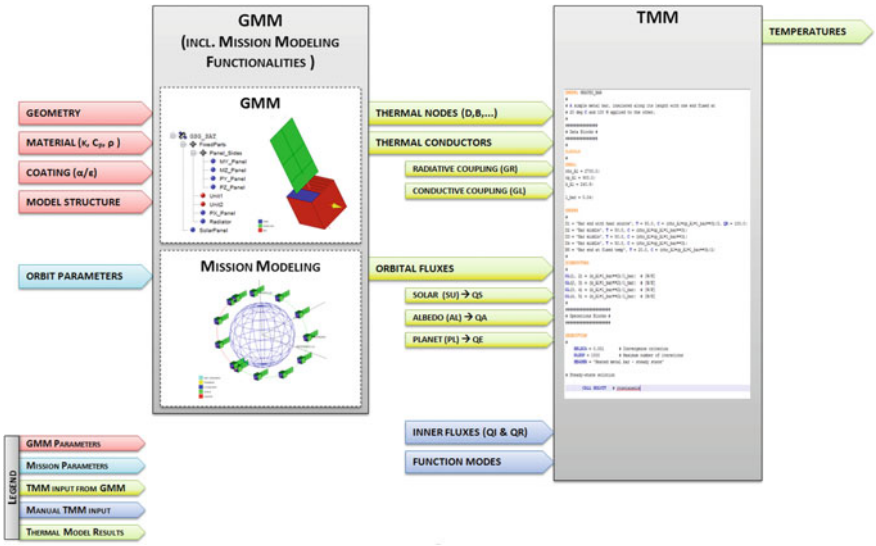

Fig. 16.11 Dependencies between geometry and mission modeling functionalities of a GMM and TMM as modeled and depictured by ESATAN-TMS

However, as soon as radiative heat couplings matter, the manual TMM setup is tiresome and error prone. In particular, for actual S/C geometries the analytical calculation of radiative couplings with their view factors is rarely feasible. In addition, a S/C usually continuously changes its orientation relative to the external environment (planet, Sun, etc.) and also the orientation between the S/C subsystems may vary (e.g. rotating solar arrays). These facts impose dynamic boundary conditions, which must be captured in the thermal network simulated by the TMM.

The generation of these elaborate radiative couplings and environmental radiative heat fluxes is the main purpose of the GMM. With evolving software capabilities the GMM nowadays is also employed to determine the environmental heat flux parameters between the nodes of the discretized system. It can also provide the thermal nodes and the conductive heat links to the TMM. All thermal nodes of a GMM then are also used in the TMM. However, not all TMM thermal nodes are represented in the GMM. From this it should be clear that it is not possible to compute temperatures of any thermal node or the entire S/C with the GMM alone. It merely provides the necessary inputs for the thermal network simulated by the TMM. It depends on the specific problem as to which parameters of the thermal network are derived from the GMM and which are included manually into the TMM by the thermal engineer.

In today's thermal engineering software packages such as ESATAN-TMS, SYSTEMA THERMICA, THERMAL DESKTOP, or NX I-deas TMG, the GMM acquires more and more abilities and thus importance as established by its graphical user interface (GUI). However, manual intervention in the TMM is still necessary to work out particular features of a S/C thermal control system, such as heater

regulation, fluid networks, or functional modes switching. Different from the GMM, which usually is handled via a graphical user interface, a list of semantic code lines is the only input to TMM calculation, which can be run in batch mode. The list can be manipulated by any text editor. The physical background, the mathematical representation, and thus the semantics for the TMM is independent of the used software package. Yet, in order to be compiled and interpreted, the TMM needs to follow a defined syntax. The syntax varies somewhat between thermal software packages. It is far beyond the scope of this book to describe differences in the syntax. The interested reader is referred to the software manuals.

Let us now have a closer look at GMM and TMM.

16.3.4 Geometric Mathematical Model (GMM)

As shown above, the GMM supports the discretization of a modeled structure into thermal nodes and CONDUCTORS. It is mainly used to determine the radiative couplings between the nodes within a S/C and between the S/C and the environmental heat sources and sinks (Sun, planets, space). However, it is also a useful method of generating the thermal nodes and the conductive heat links.

From Meshing to Thermal Network

How do we get from a given geometry of a body to the geometrical nodes? Usually, satellites are made of thin plates and foils. Therefore, in the thermal network the 3D volumetric parts of a satellite are approximated by 2D shells. The 2D shells are further discretized in 2D polygonal elements (see Fig. 16.12). The thickness of the volumetric body is represented by a parameter in the 2D polygons. The process is called *meshing*. An example of a meshed satellite is shown in Fig. 16.13. Each 2D element typically represents one thermal node. However, in most software packages it is also possible to represent multiple surfaces by just one thermal node. The nodes then contain the combined information from all the assigned surfaces, while all assigned surfaces are given the same thermal node number.

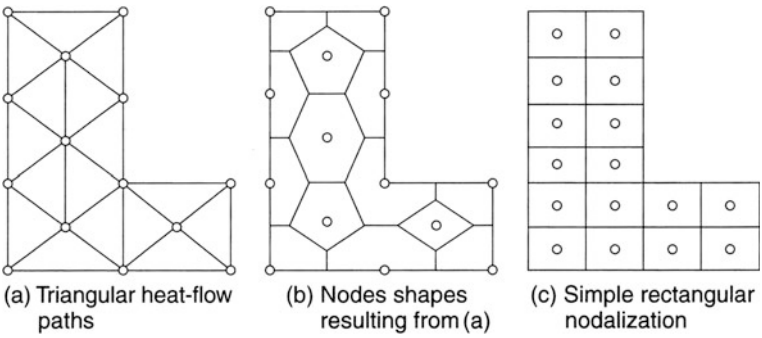

Fig. 16.12 Discretization of a 2D shell into three different types of polygonal elements that are adapted to the shell geometry. *Credit* Gilmore (2002)

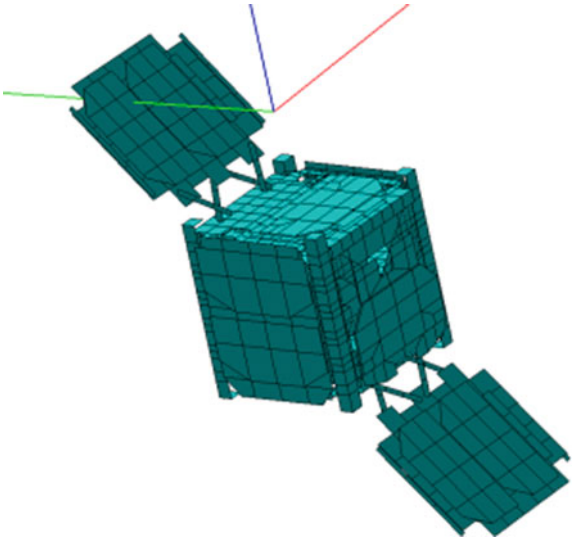

Fig. 16.13 Example geometrical mathematical model of a CubeSat

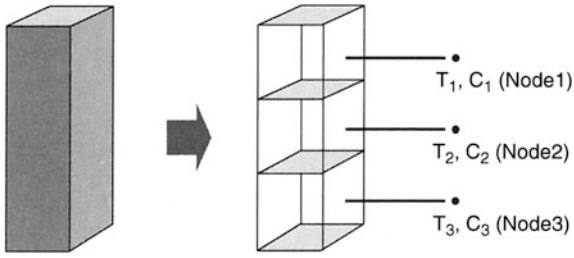

Fig. 16.14 A cuboid meshed into three thermal nodes with assigned temperatures and heat capacities. *Credit* Gilmore (2002)

For volumetric bodies some software packages offer 3D elements for more precise modeling, for example thermal isolation of cryogenic launcher upper stages. Because the vast majority of the thermal meshing is performed with 2D shells, while 3D shells are only used for rather special problems, we do not treat 3D elements in the following.

For a thermal node each assigned surface is given a specific geometry (defined by points), thickness and material (with defined specific heat and mass density). The thermal properties are then assigned to each surface to make up the corresponding thermal node (see Fig. 16.14). The heat couplings derived from the geometry establish the total conductive network between all surfaces.

In addition to the thermal nodes and conductive network, each surface of the GMM has a set of coating-dependent thermo-optical properties. These properties cover the full range of possible physical parameters. They require absorption values α and emission values ε, which can be wavelength dependent. The surfaces can be opaque or transparent and can act as diffuse Lambertian or specular reflectors. The geometrical information provided by the surface is utilized to determine the view factors $F_{t\to r}$ between the surfaces and thus between the different geometries, subsystems, etc. Here index t denotes the transmitting surface and the index r denotes the receiving surface.

With these view factors and the thermo-optical properties the radiative links between two thermal nodes are derived as given in Eq. (16.3.4). Note that it is sufficient to derive $F_{t\to r}$ while $F_{r\to t}$ can be derived according to the reciprocity relation Eq. (16.2.7). Nevertheless and even for coarse meshes a huge number of radiative links is typically generated. This results from the fact that by definition all surfaces, and as such all thermal nodes in sight of one another, are connected radiatively. Each radiative connection results in one corresponding radiative link.

In most software packages it is also possible to assign two thermal nodes (not necessarily spatially neighboring nodes) to one surface, namely the common surface of two adjacent nodes. Because each node can have a custom set of properties (type of material, thickness, thermo-optical properties), the conductive or radiative link between the nodes on different sides then is provided as a parameter of the surface. This approach is widely used to simulate surfaces covered by multi-layer isolation (MLI) blankets, or can be used for honeycomb structures.

GMM De-featuring

A GMM is typically much more simple than a geometric model for FEM. Many details are omitted, as for example bore holes or chamfers. Complicated geometric shapes are simplified, as in most cases they do not play a significant role for both the conductive and the radiative model. The process in which such geometry details are suppressed or simplified is called *de-featuring*. The amount of de-featuring and hence the fidelity level of the applied mesh strongly varies with the modeled problem and with the experience of the thermal engineer.

The GMM must at least comprise elements representing large surfaces with significant temperature differences or with a significant view factor to the external environment. Small surfaces with similar temperatures have very small radiative links to each other and therefore are negligible. However, dismissing insignificant surfaces from the GMM does not necessarily imply that the corresponding thermal nodes can be omitted from the thermal network. Those nodes and the conductive links between them can still be implemented manually in the TMM.

> **Note** *In some software packages GMM body surfaces are permitted to only conduct and not radiate to the environment. In that case they are considered to only generate thermal nodes and conductive links and do not participate in the view factor calculations.*

Unexperienced users of thermal software tend to generate large numbers of nodes without necessity. However, to reduce computation time, it is good practice to reduce the number of generated surfaces and thermal nodes as much as possible. Distributed thermal nodes are only needed when spatial temperature gradients matter. Almost isothermal surfaces should be modeled coarsely rather than finely meshed. It is the art of thermal node discretization to find the right model complexity for sensible and easily interpretable results with the lowest computation time.

GMM Node Versus TMM Node Generation

Thermal nodes can be generated in the GMM or TMM. Today, the vast majority of thermal nodes are generated in the GMM. A GMM includes at least all relevant radiative surfaces, which quite often also cover the conductive elements. However, elements which predominantly interact conductively (e.g. cables, thermal straps, heat pipes) are

typically not captured in the GMM. They are either added as thermal nodes with conductive links in the TMM or sometimes added just in the form of conductive links without an associated thermal node. A classic example are thermal straps. With their high conductivities they effectively exchange heat between the thermal nodes they connect to. But they are rarely included as thermal nodes in GMMs as their temperature rarely matters and their contribution to radiative exchange is negligible due to their small size.

For certain S/C parts, such as payloads, it is essential to capture fine-grained spatial temperature gradients and thus temperature maps to analyze thermo-elastic deformations. The GMM mesh then typically requires a higher fidelity implying more thermal nodes, the temperatures of which are transferred to finite element models to provide the required thermo-elastic deformations.

GMM and the External Environment

The basic GMM just contains the meshed geometry of the S/C, which is sufficient to establish the thermal nodes and the S/C-internal conductive and radiative network. However, as shown above, the TMM also requires boundary conditions to derive the temperatures for a given S/C mission.

Important boundary conditions are the radiative links between the S/C and the external environment, i.e. emission to space and absorption from Sun, planet IR, and albedo. These radiative links and hence heat fluxes continuously change with position and attitude of the S/C in its orbit. Because these external boundary conditions change with orbital position and S/C attitude, the GMM must be likewise adjustable. Therefore, beyond the basic GMM, which just supports the meshing of geometries, GMM software packages often also provide corresponding mission modeling functionalities. These allow the user to virtually put the S/C GMM (its meshed geometry) into an orbit around a planet or on a planetary surface. According to mission requirements, the S/C then is oriented with respect to the Sun, planet, and flight direction. Finally, the radiative heat exchange between the S/C and the external environment is derived for a finite number of sampling points in time. For every sampling point a radiative analysis is performed and the resulting radiative couplings (to space, and within the S/C) and the absorbed radiant fluxes (Sun, planet IR, albedo) are stored in lookup tables. The GMM mission modeling functionalities allow the simulation of closed orbits, chained orbital arcs, as well as open transfer trajectories with varying S/C attitudes to the external environment. The S/C attitude can be predefined, for example certain surfaces (e.g. solar arrays) are always oriented to the Sun, while other surfaces (e.g. an instrument) point to the "nadir"—to the planet.

> **Note** *In GMM the number of orbital sample points is the driving factor for the sampling frequency in the resulting TMM. Even though the TMM might utilize many more time steps over an orbit to derive the temperatures, the number of sampling points in the GMM lookup tables for the radiant flux will always limit the thermal precision over an orbit. For TMM time points in between the GMM table points, radiant fluxes will be interpolated.*

Also the external environment can be customized to some extent. For example, the thermal properties of planets can vary with orbital longitude and altitude. Some software packages also vary the planet's albedo accordingly. Also, the direction of solar radiation can be simulated to be either parallel at planetary distances or to be converging for missions close to the Sun. A recent novelty in environmental simulation is the capability to cover three body problems, such as a S/C on the surface of a planet with the Sun or moon passing over it.

A typical effect implemented in a GMM is S/C aging. S/C's thermo-optical properties usually vary (degrade) with age. Most importantly, absorptivity in the UV and visible spectrum increases with age yielding a colder S/C at the beginning and a hotter S/C at the end of a mission. Therefore, analyses are usually performed for the beginning of the mission, the so-called *beginning of life* (BOL) and for the end of the mission, the so-called *end of life* (EOL). Correspondingly, the mission feature software allows to mimic lowest (at EOL) and highest (at BOL) incident radiant fluxes by varying the solar constant as well as the albedo and the temperature of a planet. These varying thermo-optical properties of the S/C and of the external environment (Sun, albedo, etc.) are often combined to so-called *radiative cases*, to verify the thermal design of the analyzed S/C. Classically, a cold-BOL case and hot-EOL case serve as such extremes.

Monte Carlo Ray Tracing

In summary, a GMM determines the radiative heat exchange between the S/C and its environment and inside a S/C. In Eq. (16.2.4) we have seen how the radiant flux emitted from a transmitter surface and absorbed by a receiving surface is derived. Equation (16.2.19) tells us which parameters are needed to describe the radiative heat exchange between two surfaces, in particular thermal nodes. In both expressions the view factor $F_{t\to r}$ between the affected geometries (receiver and transmitter) plays a major role. In fact, it is the most difficult factor to derive, which historically was the driving force to develop GMMs. To determine view factors analytically between surfaces in 3D (cf. Sect. 16.2.2), which may even change their mutual orientation (moving parts of a S/C) and orientation (attitude) with respect to the environment (Sun, planet, etc.), would be extremely challenging and prohibitively lengthy for a S/C.

Therefore, GMMs typically utilize the numerical approach called *Monte Carlo ray tracing* (Fig. 16.15). The approach is very intuitive and can be described as follows. We first recall that the view factor $F_{t\to r}$ effectively is that fraction of the hemisphere (dome) of a transmitting plane surface, which is occupied by the receiving surface. Also remember that a typical Lambertian (diffuse) transmitter emits electromagnetic waves uniformly in all directions. These two facts are the foundation of the Monte Carlo ray tracing method.

In essence, this method simulates light beams emitted from random spots on a transmitting surface into random directions (hence the name Monte Carlo). Each beam is supposed to carry a given defined total number of emitted rays (photons). For example, if 1000 rays are fired from a sphere that emits 1 W s, each ray carries 1/1000 W s.

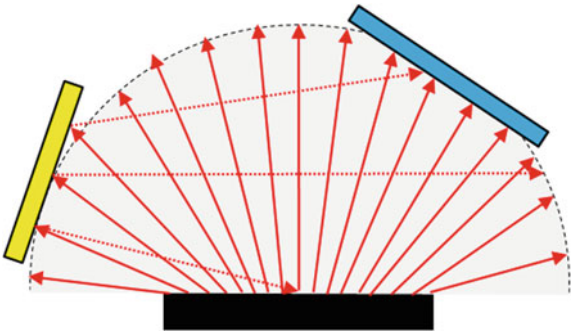

Fig. 16.15 Visualization of the Monte Carlo ray tracing method of a diffuse emitter radiating towards a blue receiver and a yellow with specular reflection

The rays "hit" absorbing surfaces that occupy fractions of the hemisphere. The Monte Carlo simulation records the angle under which a ray hits an absorbing surface (as it is part of the view factor) and according to the thermo-optical properties of the hit surface determines whether it is absorbed, transmitted, or reflected, or any combination thereof. Reflectance can be either specular or diffuse. For specular reflection the ray is simply "forwarded" according to the reflection law, while for diffuse reflections each ray becomes the source of a new ray burst of many rays carrying together the total energy remaining in the ray after the reflection.

The reflected or transmitted ray propagates further until it hits the next surface. This method allows the capturing of view factors of an emitting surface to surfaces that may not even be in direct sight. This intricate effect may be decisive for the thermal design of a S/C and is not captured with the so-called *Gebhart factor method* applied by some radiative coupling software codes.

Each ray is tracked until a given lower limit value of its virtual energy is reached, whereupon the ray is no longer considered or truncated. Overall, the ray tracer records how much energy of a given transmitter is deposited at hit receiver surfaces (direct, reflected, and transmitted rays). The view factor $F_{t\rightarrow r}$ of a receiving surface then is the total energy of all absorbed incoming rays under the corresponding angle versus the energy of all rays fired from the transmitting surface.

This approach is applied to all radiative heat exchanges between nodes within the S/C and between the S/C and the external environment. In the software the external environment is also approximated as surfaces around the S/C, however autonomously by the software not seen by the user. From the derived view factors the GMM creates radiative couplings between all surfaces and with the external environment. Because ray tracing is performed for every surface and for every orbital position and attitude of the S/C, this can result in extensive computation times and extremely big data arrays as inputs for the TMM.

To limit the data exported from the GMM to the TMM, often a filter is applied to the arrays, which removes extremely small radiative couplings. This approach, though, becomes dangerous when fine meshes are applied, because they result in a huge number

of extremely small radiative couplings. If the absolute limit then is not carefully adjusted, a noticeable error in the radiative heat exchange network may be introduced.

To further limit computation time and the size of the exported radiative couplings, the GMM of a S/C is often split in so-called *cavities*. Cavities are S/C sections, particularly inside a S/C, whose surfaces never change their orientation relative to each other and are never exposed to the external environment. Within such static cavities ray tracing need to be applied only once, while for surfaces exposed to the external environment it must be performed for any orbit position and change in S/C attitude.

16.3.5 Thermal Mathematical Model (TMM)

How are external heat fluxes, as determined by the GMM, interrelated to the internal heat fluxes due to temperature differences and to internal heat dissipation? Let us have a closer look at the Thermal Mathematical Model (TMM). In Sect. 16.3.3 we introduced the general concept behind the TMM. The TMM is a mathematical representation of the thermodynamic network, as given by the discretization of the spacecraft. This thermodynamic network consists of thermal nodes. Each thermal node in a TMM is represented by the node Eq. (16.3.5)

$$C_i \frac{dT_i}{dt} = \sum_{j \neq i} G_{ij}\left(T_j - T_i\right) + \sum_{j \neq i} R_{ij}\sigma\left(T_j^4 - T_i^4\right) + \Phi_i$$

The transient part of the thermal network is represented by the capacitors C_i of the thermal nodes, i.e. the lumped finite volumes. Their key physical parameter is the temperature T_i, which is a state variable describing the level of stored energy within a node. By definition, the temperature is constant within the volume of that thermal node. The flow of energy from one finite volume to another is driven by differing temperatures, and its amount is given by the conductive or convective, G_{ij}, and radiative, R_{ij}, coupling coefficients, which were introduced in Sect. 16.3.2. In addition, Φ_i captures heat fluxes due to internal heat sources and external heat fluxes due to the space environment.

The node equations for all nodes, which are a system of coupled linear differential equations, are key for a TMM. Several numerical solvers are available to determine the temperatures of all nodes from the node equations. Prior to solving the node equations the following steps need to be carried out for all nodes, in this sequence:

1. **Determine conductive and convective coupling coefficients** G_{ij}
   In aerospace thermal engineering, (linear) conductive coupling coefficients (CONDUCTORS) are usually denoted by $G_{L,ij}$ and convective (fluid) coupling coefficient by $G_{F,ij}$. In this book we follow the convention that G_{ij} stands for either a conductive or convective coupling coefficient.

Although the physics to determine the coupling coefficients is unequivocal, in practice many details of how the heat is transferred are vague and therefore their determination requires a lot of testing or expert knowledge. We will focus on conductive coupling coefficients here, because they occur most often. Convective coupling coefficients are only necessary for fluid loops or if heat transport in a pressurized vessel such as the ISS needs to be computed. The interested reader is referred for example to Gilmore (2002).

The thermal conductivity of a material (internal) and the CONTACT CONDUCTANCE (at the interface) between two components, although both are denoted in TMM as $G_{L,ij}$, behave physically different. The thermal conductivity of a material generally is temperature-dependent. For composite materials, such as carbon fiber reinforced plastics (CFRP), printed circuit boards (PCB), or honeycomb structures thermal conductivity can even differ significantly between different directions in the material (anisotropy), while for metals one can safely assume isotropic material properties. On the other hand, CONTACT CONDUCTANCES at the interface between conductive elements in practice vary from application to application and therefore have to be determined experimentally. Consequently, their determination is costly and hence often proprietary information of companies. More common values can be found in textbooks.

Conductive coupling coefficients and CONTACT CONDUCTANCE can be merged into one quantity in the same way as ohmic resistors in an electrical network. For n parallel conductive coupling coefficients it reads

$$G_{ij} = \sum_{n}^{1} G_{ij_n} \tag{16.3.7}$$

The according expression for n serial conductive coupling coefficients reads

$$\frac{1}{G_{ij}} = \sum_{n}^{1} \frac{1}{G_{ij_n}} \tag{16.3.8}$$

2. **Determine the radiative coupling coefficients R_{ij}**
In aerospace thermal engineering radiative coupling coefficients (CONDUCTORS) are mostly denoted as $G_{R,ij}$. In this book we however stick to our convention R_{ij}. Calculations of R_{ij} with rough values for view factors $F_{i\to j}$ and optical surface properties α, ε are a good first step to quantify radiative heat exchanges. Values for α, ε for typical thermal control surfaces are given e.g. in Gilmore (2002), Appendix A, and Sect. 16.2.6, Fig. 16.9. View factors between any pair of thermal nodes i and j can be determined analytically. For analytical expressions of view factors see for example Howell (2011), also available in the online catalog www.thermalradiation.net/indexCat.html.

Yet, with increasing complexity of the geometry (see Sect. 16.3.4), ray tracing is necessary to determine view factors and thus the radiative coupling coefficients R_{ij}. An additional complication for radiative exchanges are directional selective surfaces (see Sect. 16.1.5), a.k.a. specularity and opacity. Specularity describes the type of angular reflection (specular or diffuse) of a surface at certain wavelengths and can be temperature-dependent. Opacity is a quantity to model transmission through surfaces (transparency) in the visible part of the electromagnetic spectrum. It is cumbersome to determine specularity and opacity analytically. R_{ij} values are determined in the GMM (see Sect. 16.3.4). In the TMM the radiative coupling coefficients R_{ij} are usually provided as an external input without further processing. In principle, it is possible to manipulate R_{ij} in the TMM. This might be necessary for example to rotate S/C components, for which different sets of R_{ij} apply for different rotation states. For every time step in the TMM, for example based on the operation mode of an instrument or based on the position in orbit, an individual set of R_{ij} can be loaded by an external call.

3. **Determine internal heat fluxes $\Phi_{i,\text{int}}$**
The internal heat flux $\Phi_{i,\text{int}}$ (see Eq. (16.3.5)) generated within a node i depends on the S/C design and operational modes. It is usually caused by the heat dissipation of electronic equipment. In general and as a first approximation, it is appropriate to assume 'consumed' electric power equals 'dissipated' heat. But for a number of electronic components this statement is not true. For example, some electronic components emit a fraction of the consumed electric power in form of electromagnetic waves. Dissipated heat can also originate from exothermal chemical processes, such as the discharging of batteries or phase change of materials, as well as from radioactive decay in radioisotope thermoelectric generators (RTGs) or radioisotope heat units (RHUs). Finally, heaters, which are an electrical "equipment" to intentionally dissipate heat, are important heat sources.

   In terms of thermal modeling, the internal heat flux $\Phi_{i,\text{int}}$ can be attached to a single thermal node or a group of thermal nodes.

4. **Retrieve external heat fluxes $\Phi_{i,ext}$**
Unlike the standard notation used in Sects. 16.1 and 16.2, external heat fluxes in the TMM are usually denoted as Φ_S (a.k.a. Q_S) for direct solar heat flux, Φ_A (a.k.a. Q_A) for albedo heat flux, and Φ_E (a.k.a. Q_E) for planetary heat flux. Usually, the TMM calls them as an external input without further processing. As for radiative coupling coefficients different sets of external heat fluxes are also available, for example for a rotating part or different orbit segments. For the modeling of external fluxes see Sect. 16.3.4.

   Some thermal nodes might be exposed to environmental and/or internal heat fluxes, others not. For the node equation it is irrelevant whether a heat flux is internally dissipated heat from an electronic box or a flux from an external

source. The total heat flux on a given thermal node is always the sum of internal $\Phi_{i,\text{int}}$ and external heat fluxes $\Phi_{i,\,ext}$, whatever contributes. Therefore, for thermal nodes on the surface of a spacecraft, i.e. the boundary to space, external sources can formally be considered as neighboring nodes.

5. **Determine the heat capacity C_i for all thermal nodes i**
   The heat capacity C_i of a thermal node is its ability to store energy. It is proportional to the mass of the lumped volume and its specific heat capacity.

$$C_i = c_{p,i} m_i = c_{p,i} \rho_i V_i$$

   Determination of the node volume is straightforward and its density is a material property provided by textbooks. Be aware that there are many different types of materials such as alloys or carbon composites, each having a distinct density. Generally, the specific heat capacity is temperature-dependent and increases with increasing temperature. Values for the specific heat capacity at room temperature can also be found in textbooks or material data bases (see for example Gilmore (2002), Appendix B, or online material databases such as http://www.matweb.com). Given these values, the determination of the heat capacity (a.k.a. CAPACITANCE or thermal capacity) is usually carried out by the GMM meshing process, which forwards these heat capacities to the TMM. The temperature-dependent behavior is often more challenging to obtain. If the value of a peculiar specific heat capacity or its temperature dependence is not available, it has to be measured in dedicated material tests.

6. **Include control functionalities and variables**
   Finally, possible time-dependent heat dissipation functionalities are added to a TMM, such as a simple thermostat, a PID control logic, or the physical function of thermoelectric elements. They must reproduce the behavior of the modeled component. Also active thermal control components, such as pumped fluid loops, can be modeled and included in the TMM.

   Another feature of TMMs is the possibility to include variables to parameterize the model. This allows switching between operational modes or the study of the impact of single parameters on the results of the entire model.

The set of node Eq. (16.3.5) is finally solved with a standard finite difference method. The solution provides the temperatures of all nodes of the modelled body. A mistake commonly made by inexperienced thermal engineers is to thoughtlessly accept the results as a given fact. Results may look credible, although the numerical solvers have not converged to the given limit. So, a check whether the convergence criteria of the solver are achieved is always in order. Be critical with the temperature results you obtain and don't fall in love with your model—be self-critical.

16.3.6 Applied Thermal Design and Analysis

We have seen above that S/C thermal design is analyzed by a discretized thermal model with many thermal nodes. Thus the thermal behavior of a real satellite, i.e. its temperatures at different orbital positions and attitudes is determined. Analytical considerations (see Sect. 16.2) can provide only a very basic idea of the average temperatures of entire bodies at special orbital conditions. In this chapter we examine how a discretized thermal model must be set up and which kind of analyses are necessary at which levels. At the end, the vital question is tackled of how precise thermal models and their temperature predictions can be and how the remaining temperature uncertainties are handled to obtain robust and reliable results.

Global Versus Local Analyses

Thermal design of an entire satellite is usually broken down into a subset of smaller thermal design problems. On the other hand S/C subsystems or units with similar temperatures are usually merged into a so-called *temperature enclosure,* which is then designed to attain the predefined temperature.

To create local enclosures, local thermal design methods are applied to balance, couple, or isolate the enclosures from each other. The task of the thermal engineer then is to balance the heat flows between the different enclosures in such a way as to maintain the desired temperatures throughout the mission in each of them. This is commonly achieved by thermal control hardware such as: distributed heater patches, heat pipe networks, customized MLI blankets, or thermally isolating washers or thermal fillers for interfaces.

As in other disciplines thermal engineering also applies a combination of global and local analyses, which are often, but not always, split over different contractual levels. Global analyses are utilized to check the compatibility of the overall thermal design with mission requirements and to check interface temperatures between the S/C and all its subsystems by means of temperature reference points (TRPs). TRPs are selected locations within a S/C in particular within a subsystem, at which the global analysis guarantees a given temperature. This information is used by the local analysis as a boundary I/F temperature.

Local analyses are performed on subsystem and on component level in environments derived from global analyses. Depending on the complexity of the subsystem, multiple levels of local analyses can be necessary to justify a given thermal design. On the component level this can lead to thermal meshes with a very high number of thermal nodes. At all levels, the critical cases that drive the thermal designs of components or subsystems may be quite different.

Capturing Spatial Temperature Gradients

For a subsystem, temperature requirements dictate the temperature range for all parts, including all hot and cold spots. Thermal models with too few nodes, down to one node per subsystem, can provide a first estimate of the scale of temperatures to be expected. But they fail to reliably predict the temperatures for any location of a modeled subsystem because they average out extreme temperatures. So, to capture

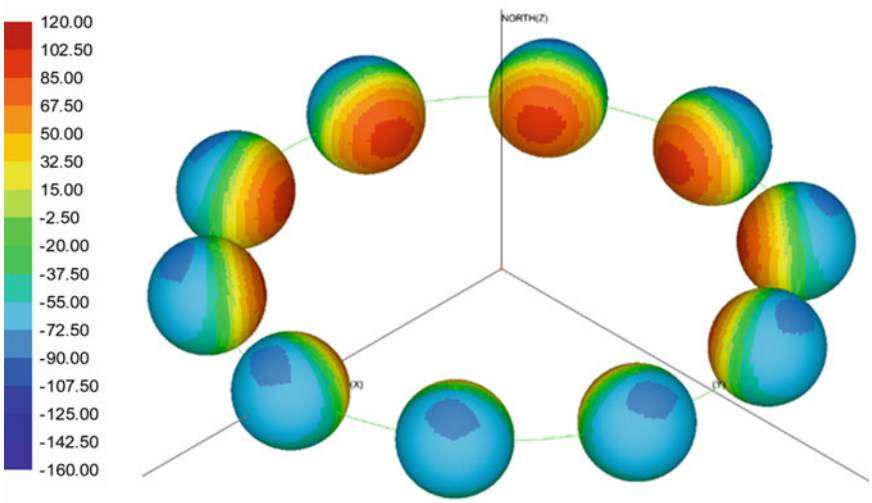

Fig. 16.16 Temperatures of perfectly black titanium sphere (thin shell with thickness 5 mm) circling the Sun in 1 AU distance. The sphere is discretized with 80 × 80 thermal nodes. Analysis and visualization by ESATAN-TMS

all the corresponding temperature gradients, a large number of thermal nodes must be employed.

Consider a black sphere (shell of 5 mm thickness) of titanium as a modest example of a satellite circling the Sun at distance of one astronomical unit (1 AU) as shown in Fig. 16.16. Thermal analysis with 80 × 80 thermal nodes reveals that it would experience temperatures in the range of +110 °C (facing the Sun) to −90 °C (facing space), while a global analytical heat balance analysis by a one-node model would suggest an average temperature of roughly +15 °C. This mean temperature would satisfy the typical permissible operational temperature range of +10 to +30 °C of a battery. However, in reality mounting the battery at any location within the S/C shell, would heavily violate the temperature limit. This simple example justifies why a certain minimum level of discretization is necessary even in the most global S/C thermal analysis. The discretization approach explained in Sects. 16.3.4 and 16.3.5 for the GMM and TMM provides the means to model such details.

Capturing Temporal Temperature Gradients

For most missions the S/C environment around a planet or on a planet's surface, that is the solar, albedo, and IR heat fluxes changes continuously. To capture all the transient temperature gradients of a S/C and to identify the most extreme thermal conditions, multiple points in time must be analyzed. Too few points may miss temperature extremes thus providing only approximate results. To properly capture transient temperature effects GMM and TMM must be set up with respective temporal granularity.

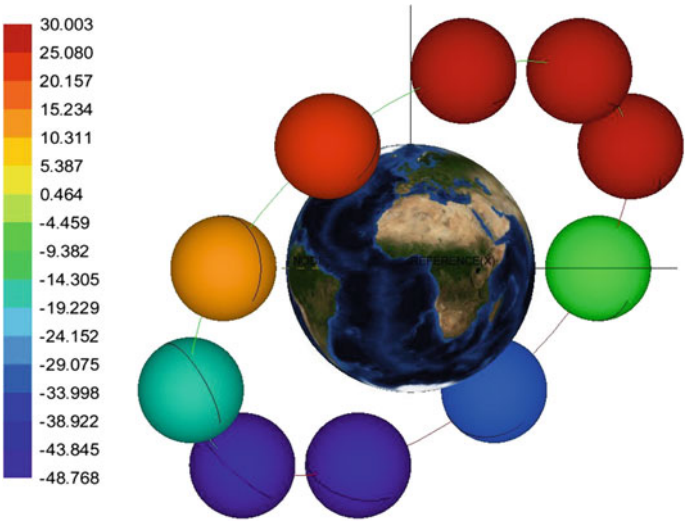

Fig. 16.17 Temperature evolution of perfectly black titanium sphere (shell with thickness 5 mm) in an ISS orbit (altitude 400 km, inclination 51.6°) around Earth. The sphere is modeled with one thermal node. Analysis and visualization by ESATAN-TMS. Sphere and orbit dimensions are not to scale

Therefore, in the GMM it is essential to ensure that not only critical transitions or attitude changes that strongly affect the heat fluxes (e.g. entry into eclipse) are covered in the analysis, but also that the gradual phases between those fast transitions are sampled with reasonable granularity. These rapid cases are then fed into the TMM to derive the temperature changes of a S/C over an orbit or along a trajectory. The TMM also requires the time history of the internal fluxes (e.g. heaters, electronic box heat dissipations) in order to cover the heat balance fluctuation caused by operational modes.

Consider again our battery with a temperature limit of +10 to +30 °C. If the local environment of the battery, that is for example the temperature of a dedicated compartment inside the S/C, changes evenly over an orbit between −20 and +60 °C, the average temperature of the battery would be +20 °C. This favorable temperature, however, would rarely occur. Most of the time the temperatures would violate the allowable upper and lower limits, which implies a failed thermal design.

Figure 16.17 shows the mean temperatures of a black sphere of titanium (shell of 5 mm thickness) circling Earth in an ISS-type orbit at different locations on its orbit. The temperature is maximal +30 °C on the dayside and minimal −48 °C on the nightside. Therefore, to capture such a temperature evolution, thermal analysis needs to be done at multiple points along the S/C trajectory.

In summary, for a reasonable temporal and spatial temperature profile a thermal model with multiple nodes and at multiple points along the trajectories is required as shown in Fig. 16.18.

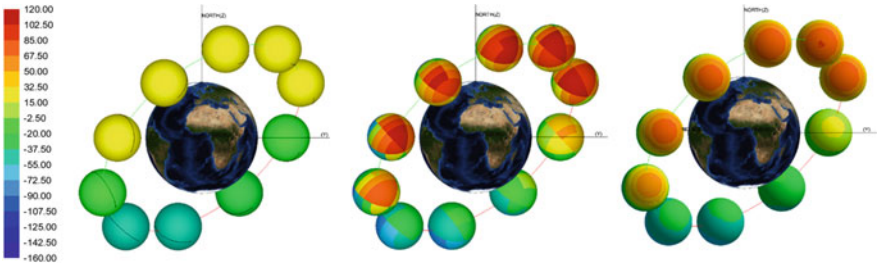

Fig. 16.18 Temperature evolution of a perfectly black titanium sphere (shell with thickness 5 mm) in an ISS orbit (altitude 400 km, inclination 51.6°) around Earth. The sphere is discretized with one (left), 6 × 6 (center) and 80 × 80 (right) thermal nodes, highlighting the impact of different orbital positions and of different spatial discretizations. Analysis and visualization by ESATAN-TMS. Sphere and orbit dimensions are not to scale

> **Note** *Most thermal analysis software packages offer the option to calculate time averaged temperatures in a so called "steady-state" mode. Caution is required when using this mode. It typically is used to establish initial temperature figures for subsequent transient analyses, and for this purpose it can be a suitable tool. For most missions it is useless for verifying the thermal design versus the thermal requirements because the steady-state hides all transient variations in the temperature.*

Spacecraft Lifetime Considerations

Space missions typically last several years. The degradation of the S/C and the change of the environment over such a long period must be considered in any thermal analysis. Most importantly, the S/C coatings degrade as discussed in Sect. 16.2.6. Also electronic components age in that they dissipate more heat as their electrical efficiency declines, primarily due to the total ionizing radiation dose received.

Also the environment changes over a mission, particularly for interplanetary missions. Consider for example a probe to Jupiter. At its final destination far away from the Sun the thermal design is all about keeping it warm, which often requires small heater units and MLI blankets on the S/C hull with outer layers having a high alpha/epsilon. Jupiter missions, however, initially often journey through the inner solar system to pick up speed by gravity assist maneuvers at inner planets, such as Venus. So close to the Sun the S/C needs to be shielded against the excessive solar heat flux. This is usually achieved by using a white coated high gain antenna as a solar shield.

Even in planetary orbits environmental changes are significant. In Earth orbit the variation of the solar declination from +23.5° to −23.5° over one year, the distance between Earth and Sun caused by the slightly elliptic orbit of the Earth, as well as the change in solar flux caused by the eleven year solar cycle lead to considerable variations in the environmental heat fluxes.

All these changes over a mission lifetime must be covered by thermal analyses in order to demonstrate that the thermal design is robust and that the thermal control system is able to meet the requirements at all times.

Worst-Case Analysis

Despite the need to provide the temperature information over an entire lifetime of a satellite, it is currently impracticable to simulate the entire mission duration. This would require numerical simulations yielding immense quantities of data, which subsequently have to be post-processed and interpreted. In order to limit the number of evaluated cases to a manageable number only so-called *worst case scenarios* are considered, which are the extreme cases of all possible environment and S/C combinations. Classically, the worst hot and worst cold case are established to predict extreme S/C temperatures. These cases are often associated with a certain phase of the mission.

In the worst cold case the lowest temperatures of a S/C are predicted and under nominal conditions the required heater power is derived. In addition, the worst cold case is often merged with the beginning of life (BOL) conditions. At the beginning of a mission the $\alpha_{sol}/\varepsilon_{IR}$ of the outer coatings is lowest (see Fig. 16.9) and hence the S/C coldest. The worst hot case predicts the highest S/C temperatures. It is merged with the end of life (EOL) conditions, as here the $\alpha_{sol}/\varepsilon_{IR}$ and the electrical components' heat loss are highest.

Take for example a classical thermal design of an electronic unit mounted on a radiator and equipped with heaters for temperature control. The worst-case analysis is as follows:

- The thermal design starts with the worst hot case, applying EOL conditions. This case is used to size the radiator for the highest heat loads.
- The worst cold case is established with the radiator set to the BOL conditions, to check the temperatures resulting from minimum heat loads and with the radiator sized to the maximum heat loads. This case determines if heating of the controlled item is necessary and if so, how much heater power is required.

The typical worst cases mentioned above are a minimum set of analyses, but it is not by any means sufficient to cover all contingency cases. In addition, S/C temperatures and/or heater power demands must also be determined for different operation modes (e.g. safe mode, communication mode, etc.) and mission scenarios (attitude changes, orbital maneuvers, launch and early operations phase, etc.).

Generally, the definition and description of a few example cases as a surrogate for the entire mission scenario is one of the most difficult tasks in thermal engineering and requires a significant level of experience.

Modeling Uncertainty

No mathematical model is absolutely exact. This is a result of all the simplifications that are part of the modeling process and the inherent inaccuracies of the many detailed properties of thermal hardware. So the question is: How precise is a thermal analysis and how much does it err? The answers to this question is key for

the reliability of thermal analyses as a part of the thermal design verification chain of a S/C. The reliability depends, of course, on the quality of the modeled S/C and of the modeled environment, in which the S/C operates or is tested. The simplifications and inaccuracies mentioned above are combined in the so-called *(thermal) modeling uncertainty*.

The so-called *calculated temperature range* (see Fig. 16.19) is the combination of the most extreme temperatures determined by all thermal analyses. The modeling uncertainty (i.e. the known or assumed inaccuracies of the model) is added to this range yielding the so-called *predicted temperature range*.

Modeling uncertainty is the upshot of uncertain bulk material properties or uncertain thermo-optical surface properties, interface conditions, geometrical details, and thermal control settings.

Uncertainties of bulk material properties result from deviations from assumed properties or from unknown or disregarded anisotropic material properties. Thermo-optical surface properties strongly vary with the substrate material or surface treatment (coating) applied to the surface. In addition, wavelength dependencies, diffuse and specular reflectivity, and the opacity of coatings usually are not or are only insufficiently modeled. Uncertain details about physical contacts between adjunct parts cause interface uncertainties. Applied geometrical model simplifications cause GMM uncertainties. In addition, uncertain heater locations, thermistor tolerances, and unknown PID control settings bring about thermal-control uncertainties. Another common source of uncertainty is the varying efficiency of MLI, which often is only known for flat samples. MLI edge effects and the folding round edges can significantly degrade blanket performance. In addition to S/C-related inaccuracies and uncertainties, environment uncertainties can also lead to variations in the model results.

The modeling uncertainty is typically obtained by running multiple sensitivity analyses for a specific thermal case. In each sensitivity analysis the S/C or the environmental parameters are varied within their inaccuracy ranges. In practice, sensitivity analyses are often performed only for the worst hot and cold cases or

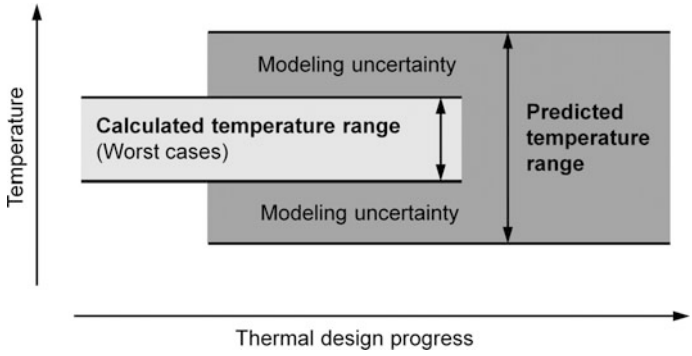

Fig. 16.19 Terminology in thermal analysis for temperature ranges and (thermal) modeling uncertainty, based on the uncertainty approach for thermal control system (TCS) used by the European Space Agency. Adapted from ECSS-E-ST-31C

Table 16.1 Exemplary values for thermal model parameter uncertainties

Class	Parameter	Inaccuracy
Environmental	Solar intensity	± 21 W/m^2
Physical	Absorptivity	± 0.1
	Emissivity	± 0.03
	Dissipation (for absolute value <10 W)	$\pm 10\%$
Geometrical	Shape (view) factors (simple geometry)	$\pm 10\%$

Credit ECSS

sometimes even only for one of these cases, while the resulting uncertainty then is applied to all cases.

A list of model quantities to be varied and recommendations on the variation ranges can be found for example in ECSS-E-HB-31-03A. The values given in this ESA reference are based on the experience of thermal engineers and analysts in the European space industry from numerous missions. In Table 16.1 a couple of typical model parameter uncertainties are shown. The full list can be found in ECSS-E-HB-31-03A, Sect. 6.5.

Due to the large number of nodes in thermal models, it is often impractical to derive the modeling uncertainty for each thermal node. Instead, for each subsystem and component representative nodes are identified, for which the modeling uncertainty is calculated. Those representative nodes can be, for example, the temperature reference points (TRP) or nodes representing a particularly sensitive piece of equipment. For each representative node the result of the sensitivity analysis is the root mean square (RMS) of all temperature deviations of the different parametric analysis runs (see ECSS-E-HB-31-03A).

In a last step, the modeling uncertainty, as given by the RMS, is applied to both sides of the *calculated temperature range* of each component: It is subtracted from the coldest temperatures and added to the hottest ones, thus widening the temperature range. This extended temperature range is the 'predicted' temperature range.

In early design phases the modeling uncertainty is often determined by experience or is based on standardized values. As the thermal design and thermal model matures, it is later replaced by modeling uncertainty values, derived by the aforementioned sensitivity analyses. As soon as the thermal design is tested and the measured temperatures become available, the thermal model is typically correlated against the test results, and the modeling uncertainty range can be further reduced.

The domain of thermal S/C modeling ends here, however not that of thermal design. The S/C and its subsystems and components still needs to be tested to qualify for orbital operations. In order to add reliability to the design, these tests are done at more extreme temperatures than those expected in orbit. Additional margins are applied in thermal tests to increase the reliability of the system. Yet, thermal testing and the system level verification process is beyond the scope of this book.

16.3.7 Case Studies

In order to illustrate how thermal modeling works, we present a simple example: a heated bar made of a metal is assumed to behave as a gray body in Low Earth Orbit. The heated bar is modeled by three diffusive thermal nodes along the x-axis (see Fig. 16.20) numbered 1, 2, and 3 and one boundary node 4.

Case 1
We make the following assumptions:

(a) The heated bar is assumed to circle Earth at 400 km altitude.
(b) All nodes are cubes and have equal edge lengths $l = 10$ cm.
(c) All nodes are made of aluminum with $\kappa_{alu} \approx 160$ W m^{-1} K^{-1}.
(d) Node 1 is exposed to the Sun on its $-x$-side, which has black paint properties $\varepsilon_{1,IR} = 0.9$ and $\alpha_{1,sol} = 0.9$ (see Fig. 16.9).
(e) Node 1 and 2 are covered with a perfectly isolating insulation on all $+/-y$ and $+/-z$ sides, i.e. these sides are adiabatic.
(f) Node 3 sides are not insulated, but covered by a SSM coating with properties $\varepsilon_{3,IR} = 0.9$ and $\alpha_{3,sol} = 0.1$ (see Fig. 16.9).

The boundary conditions for the computation are:

(I) The mean solar irradiance (solar constant) is $E_{sun} = 1361.5$ W m^{-2}.
(II) There is a constant internal heat source in node 2 of $\Phi_{2,\text{int}} = 2$ W.
(III) The boundary node 4 represents Earth, which is a black-body radiator with $T_{earth} = 255$ K.
(IV) The background temperature of space is $T_\infty = 2.7$ K.

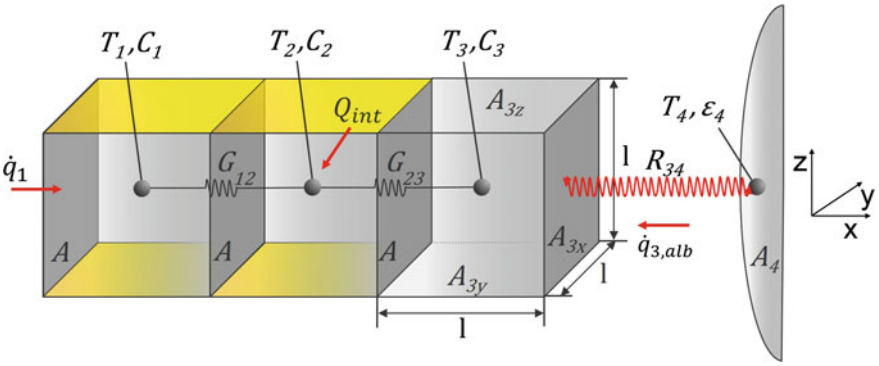

Fig. 16.20 A heated bar in LEO oriented to nadir. The bar is modeled by three cubes (nodes) with equal volumes. Shown is the conductive path through the solid material and the radiative exchange between two end surfaces

Geometry

$$A_{123,xyz} = l^2$$
$$V_{123} = l^3$$

Applying Eq. (16.2.10) for the view factor we have

$$F_{3x\to 4} = \mu^2 \cos\phi \quad \text{with } \phi = 0^\circ$$

and for the view factor of the surfaces A_{3y} and A_{3z} perpendicular to a sphere we can use (Howell 2011)

$$F_{3z\to 4} = F_{3y\to 4} = \frac{1}{\pi}\left(\arctan\frac{\mu}{\sqrt{1-\mu^2}} - \mu\sqrt{1-\mu^2}\right)$$

with $\mu = R/(R+h)$, where R is Earth's radius, and h orbit altitude above the Earth's surface. The view factor of the surfaces A_{3y} and A_{3z} to deep space (∞) can be derived from the summation rule Eq. (16.2.6) and the reciprocity relation, Eq. (16.2.7)

$$F_{3z\to\infty} = 1 - F_{3z\to 4}$$
$$F_{3y\to\infty} = 1 - F_{3y\to 4}$$

The view factor between the surface facing away from the Earth to deep space can be assumed to be

$$F_{1x\to\infty} = 1$$

From the geometry and the assumptions we can derive the following conductive and radiative CONDUCTORS

$$G_{12} = G_{23} = \frac{\kappa_{alu}A}{l} = \kappa_{alu}l$$
$$R_{3x\to 4} = \alpha_{4,IR}\varepsilon_{3,IR}A_{3x}F_{3x\to 4} = \varepsilon_{3,IR}A_{3x}F_{3x\to 4}$$
$$R_{3y\to 4} = R_{3z\to 4} = \alpha_{4,IR}\varepsilon_{3,IR}A_{3y}F_{3y\to 4} = \varepsilon_{3,IR}A_{3y}F_{3y\to 4}$$
$$R_{1x\to\infty} = \varepsilon_{1,IR}A_{1x}F_{1x\to\infty} = \varepsilon_{1,IR}A_{1x}$$

From the material properties we can derive the CONDUCTORS for transient calculations:

$$C_i = c_{p,i}\rho_i V_i, \quad i = 1,2,3$$

The boundary condition for node 1, i.e. the node exposed to the Sun, is

$$\Phi_{sun\to 1} = \alpha_{1,sol}A_1 E_{sun}$$

For node 3 there is an albedo heat flux from the Earth, which can be written as

$$\Phi_{4\to 3,\,alb} = \alpha_{3,\,sol} E_{sun} a \left(A_{3x} F_{3x\to 4} + 4 \cdot A_{3y} F_{3y\to 4}\right)$$

where $a = 0.3$ is Earth's albedo. Finally, we have the Earth's radiation at infrared wavelengths to node 3, which is addressed by the term

$$\Phi_{4\to 3,\,IR} = \left(R_{4\to 3x} + 4 \cdot F_{4\to 3y}\right)\sigma\left(T_4^4 - T_3^4\right)$$

where $R_{4\to 3x} = \alpha_{3x,y,IR}\varepsilon_{4,IR} A_4 F_{4\to 3x,y}$. Because we assume Earth to be a black body radiator, we have $\alpha_{4,IR} = \varepsilon_{4,IR} = 1$. Because we also assume the heated bar surface behaves as a gray body, we have from Eq. (16.1.35) $\varepsilon_{3y,\,IR} = \alpha_{3y,\,IR}$ and therefore

$$\alpha_{3y,\,IR}\varepsilon_{4,\,IR} = \alpha_{4,\,IR}\varepsilon_{3y,\,IR}$$

With the reciprocity relation (16.2.7) we therefore have

$$R_{4\to 3x} = \alpha_{3,\,IR}\varepsilon_{4,\,IR} A_4 F_{4\to 3x} = \alpha_{4,\,IR}\varepsilon_{3,\,IR} A_3 F_{3x\to 4} = R_{3x\to 4}$$
$$R_{4\to 3y} = \alpha_{3,\,IR}\varepsilon_{4,\,IR} A_4 F_{4\to 3y} = \alpha_{4,\,IR}\varepsilon_{3,\,IR} A_3 F_{3y\to 4} = R_{3y\to 4}$$

and therefore

$$\Phi_{4\to 3} = \left(R_{3x\to 4} + 4 \cdot R_{3y\to 4}\right)\sigma\left(T_4^4 - T_3^4\right)$$

In summary, we can write the transient node equation, Eq. (16.3.5) for each of the three thermal nodes:

$$\text{Node 1: } c_{p1}\rho_1 V_1 \frac{dT_1}{dt} = G_{12}(T_2 - T_1) + R_{1x\to\infty}\sigma\left(T_\infty^4 - T_1^4\right) + \Phi_{sun\to 1}$$

$$\text{Node 2: } c_{p2}\rho_2 V_2 \frac{dT_2}{dt} = G_{12}(T_1 - T_2) + G_{23}(T_3 - T_2) + \Phi_{2,\text{int}}$$

$$\text{Node 3: } c_{p3}\rho_3 V_3 \frac{dT_3}{dt} = G_{23}(T_2 - T_3) + \left(R_{3x\to 4} + 4 \cdot R_{3y\to 4}\right)\sigma\left(T_4^4 - T_3^4\right) + \Phi_{alb\to 3}$$

Case 2
We invert the optical surface properties, i.e. set the front of node 1 to black paint and the outer surfaces of node 3 to SSM.

Case 3
We vary Case 1 and assume that the internal cross section area between nodes 1, 2 and 3 is reduced to 10%.

$$G_{12} = G_{23} = \frac{\kappa_{alu} 0.1A}{l}$$

The area in radiative exchange with the Sun, space and Earth remains the same as in Case 1.

Table 16.2 Steady state temperatures for nodes 1, 2, and 3 for Cases 1–5

Case	Description	T_1 [°C]	T_2 [°C]	T_3 [°C]
1	Reference	11.99	12.06	11.95
2	Inverted optical surface properties	28.97	28.45	27.75
3	Reduced cross-section, reduced G_{ij}	81.73	82.04	80.55
4	Titanium material properties	12.73	14.52	11.83
5	Transient case with eclipse half or the orbit	−42.88	−42.81	−42.92

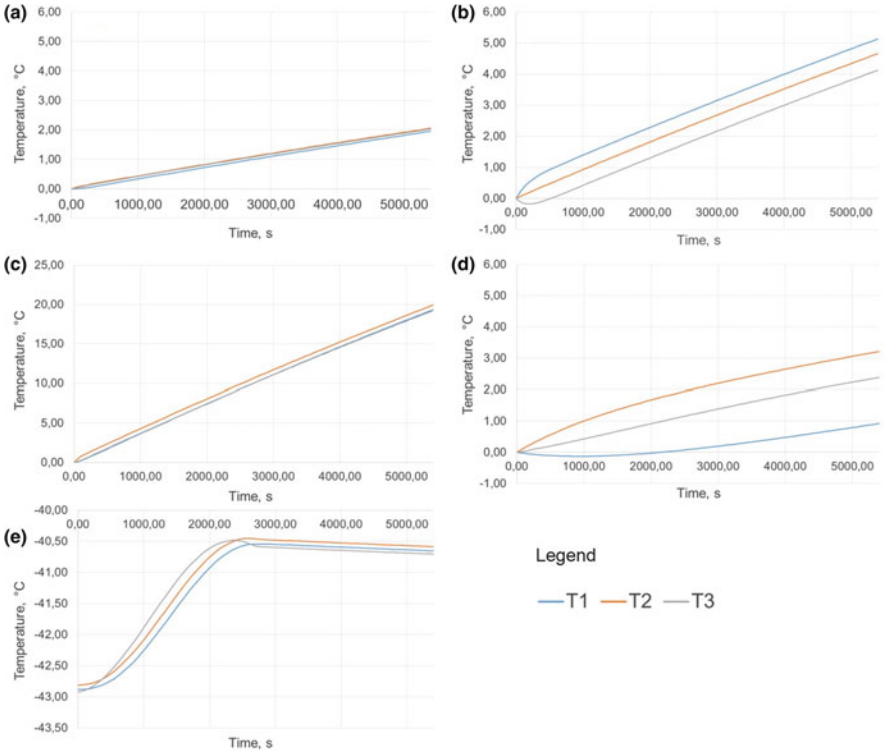

Fig. 16.21 Transient temperatures for nodes 1, 2 and 3 for cases 1–5. Initial temperature 0.0 °C except for figure **e**: **a** bar made of aluminum; **b** bar made of aluminum, but inverted optical surface properties; **c** bar made of aluminum with 10% cross section area; **d** bar made of titanium; **e** bar made of aluminum with an eclipse phase and a sinusoidal sun and albedo heat flux, initial temperature of −42.8 °C

Case 4

We vary Case 1 and use titanium material properties instead, $\rho_{Ti} = 4430$ kg m^{-3}, $c_{p,Ti} = 540$ J kg^{-1} K^{-1}, $\kappa_{Ti} = 6.7$ W m^{-1} K^{-1}.

Case 5
We look at the transient behavior of case 1 starting at an initial temperature of $T_{i,t=0} = 0.0\,°\text{C}$, $i = 1, 2, 3$. Furthermore we vary E_{sun} in a sinusoidal way, assuming an orbit period of 90 min and include an eclipse duration for half the orbit. We also assume that albedo follows a sinusoidal change in intensity, only on the dayside of the orbit.

The thermal results of cases 1-5 are given in Table 16.2 and Fig. 16.21.

16.4 Problems

Problem 1 *Wien's Displacement Law*
Prove Wien's displacement law Eq. (16.1.20) from Planck's law Eq. (16.1.19).

Problem 2 *Earth's IR Radiation*
According to Sect. 16.2.3 the solar irradiance at Earth on average is 1361.5 W m^{-2}. Show from applying Eq. (16.2.24) that the absorption of this radiation with an average albedo of $a = 0.31$ causes a radiated thermal energy that is equivalent to that of a black body radiator temperature of $T = 254$ K.

Problem 3 *Hot and Cold Cases of a Satellite in LEO*
A spherical satellite without any internal heat source is circling Earth in LEO at an altitude of 400 km. Consider the satellite as a body in full thermal equilibrium with its environment and Eq. (16.2.28) applies.

(a) Show that in the so-called *hot case*, where $\delta_{sun} = \delta_a = 1$, a change from a gray surface, $\alpha_{sol}/\varepsilon_{IR} = 1$, to a surface coated with zinc oxide, $\alpha_{sol}/\varepsilon_{IR} = 0.22$, yields a body temperature decrease of roughly 78 °C.
(b) Show that in the so-called *cold case* (nightside), where $\delta_{sun} = \delta_a = 0$, such a change of surface material does not have any effect on body temperature!
(c) Show that in the hot case the satellite with a gray surface would be cooler by 24 °C if Earth's albedo would be absent.

Literature

Baehr, H.D., Stephan, K. (2006). *Heat and Mass Transfer*, 2nd ed, Springer Verlag, Berlin, Heidelberg, ISBN 978-3-540-29526-6
Clawson, J.F., et al. (2002). *Spacecraft Thermal Environments*, in Spacecraft Thermal Control Handbook, Vol I, (D.G. Gilmore, ed.), p. 21–69
ESA PSS-03-108 (1989). *Spacecraft Thermal Control Data*
ECSS-E-ST-31C (2008). Thermal Control General Requirements
ECSS-E-HB-31-03A (2016). Thermal Analysis Handbook
ESATAN-TMS (2010), Thermal Engineering Manual (Whetstone, Leicester, UK), ITP Engines

Gilmore, D.G. (2002), Spacecraft Thermal Control Handbook, Volume I: Fundamental Technologies, 2nd edition, El Segundo, California 90245-4691, Aerospace Corporation Press, ISBN: 978-1-88498911-X

Howell, J.R., R. Siegel, M.P. Mengüc (2011). *Thermal Radiation Heat Transfer*, 5th ed., CRC Press, ISBN 978-1-4398-0533-6

Incropera, F.P., DeWitt, D.P., Bergmann, T.L., Lavine, A.S. (2013). *Principles of Heat and Mass Transfer*, 7th ed, John Wiley & Sons, Singapore Pte. Ltd, ISBN 978-0-470-64615-1

Rohsenow W.M., Cho, Y.I, Hartnett J.P. (eds.) (1998). *Handbook of Heat Transfer*, McGraw-Hill Education Ltd, ISBN 978-0070535558